INL/RPT-22-67512

Fabrication and Characterization of Candidate Alloys for Advanced LEU Fuel Concepts

May 2022

Laura Sudderth
Cynthia Adkins
Mason Childs
Scott Anderson

Idaho National Laboratory

INL is a U.S. Department of Energy National Laboratory
operated by Battelle Energy Alliance, LLC

INL/RPT-22-67512

Fabrication and Characterization of Candidate Alloys for Advanced LEU Fuel Concepts

Laura Sudderth
Cynthia Adkins
Mason Childs
Scott Anderson

May 2022

Idaho National Laboratory
Advanced Fuel Manufacturing and Development
Idaho Falls, Idaho 83415

http://www.inl.gov

Prepared for the
U.S. Department of Energy
Office of National Nuclear Security Administration
Under DOE Idaho Operations Office
Contract DE-AC07-05ID14517

Page intentionally left blank

ABSTRACT

A set of novel uranium-based alloys has been proposed for use in advanced LEU fuel systems. This study seeks to develop methods to fabricate single-phase alloys and evaluate the compatibilities of the alloys for use in composite fuel systems. The as-cast microstructure of each alloy was characterized via scanning electron microscopy (SEM), and candidate alloys were further down-selected for homogenization and interaction testing. The $U_{22}Zr_{20}Nb_{58}$ alloy was successfully fabricated as a single-phase system, as demonstrated via X-ray diffraction (XRD) and SEM. The thermal and mechanical properties of the U-Nb-Zr alloy were further assessed via differential scanning calorimetry (DSC), laser flash analysis (LFA), and Vickers' micro-hardness testing. This alloy also demonstrated improved compatibility with fuel candidate alloys from conventional matrix materials and may be a viable option for use in advanced fuel systems.

Page intentionally left blank

CONTENTS

FIGURES

TABLES

Page intentionally left blank

ACRONYMS

RERTR	Reduced Enrichment for Research and Test Reactor program
HPRR	High Performance Research Reactor program
LEU	Low Enriched Uranium
ALEU	Advanced LEU program
FAST	Fission Accelerated Steady-state Test
ATR	Advanced Test Reactor
BCC	Body-Centered Cubic
SEM	Scanning Electron Microscopy
XRD	X-Ray Diffraction
BSE	Backscattered Electron
EDS	Energy Dispersive Spectroscopy
LFA	Laser Flash Analysis
DSC	Differential Scanning Calorimetry

Page intentionally left blank

Fabrication and Characterization of Candidate Alloys and Interaction Behaviors for Advanced LEU Fuel Concepts

1. INTRODUCTION AND BACKGROUND

Dispersion fuels are of interest in high power reactors due to high retention of fission products. Concepts incorporating a fuel into a non-fissile matrix have been developed under the Reduced Enrichment for Research and Test Reactors (RERTR) and High-Performance Research Reactor (HPRR) programs [1,2]. Uranium-molybdenum alloys have been extensively studied under these programs for low temperature, non-power producing applications that utilize low-enriched uranium (LEU), which is uranium of less than 20% U-235 concentration. While these fuels exhibit improved heat transfer and irradiation behavior [3], the reduced fissile material density also reduces the potential reactivity in the reactor.

The reduction in fissile material density can be overcome by increasing the uranium density in the fuel, while still utilizing LEU. Proposed alloy concepts include U_3Si and alloys with low concentration of Mo and Si (U-1Mo-2Si, U-2Mo-1Si) [4].

Another option to improve the fissile material density is to utilize an alloy containing fissile atoms as the matrix material. A uranium alloy containing Nb and Zr ($U_{22}Zr_{20}Nb_{58}$, U-43.28Nb-14.65Zr, wt%) was proposed due to the desirable thermal properties of Nb and Zr and the body-centered cubic (BCC) crystal structure of the alloy [5], providing the alloy with isotropic swelling and higher thermal conductivity.

In order to fully utilize the benefits of these advanced fuel concepts, single-phase alloys must be developed. The bulk material properties of the candidate alloys have also not yet been sufficiently evaluated for predicting and understanding their irradiation behavior. This study was performed to characterize the as-fabricated microstructural, thermal, and mechanical properties of the alloys.

Along with characterizing the bulk material properties, it was necessary to evaluate the interaction behavior between the novel fuel (U-xMo-ySi) and matrix (U-43.28Nb-14.65Zr) candidates and compare to common fuel (U-xMo) and matrix (Zr) candidates. The Advanced LEU- Fission Accelerated Steady-state Test (ALEU-FAST) in the Advanced Tests Reactor (ATR) was used as the temperature basis for this experiment, with target fuel temperatures of 300-500ºC. These interaction tests were performed between each of the fuel and matrix candidates slightly above the temperature range intended for operation. Additional tests were performed at elevated temperatures in order to better predict potential complications that may be introduced due to power and temperature fluctuations during irradiation testing. This report summarizes the alloy characterization and the results of the initial testing of the pre-irradiation behaviors of U-xMo-xSi, and U-43.28Nb-14.65Zr alloys.

2. EXPERIMENTAL

Advanced alloy testing initiated with the development of a method to fabricate the novel fuel compositions and microstructural characterization of the as-cast material. Next, heat-treatment tests were performed on bulk material castings to improve the homogenization of the alloys. Thermal and mechanical property assessments were also performed to better characterize the behavior of the bulk alloys and predict the irradiation behavior. Temperatures for interactions testing were selected based on the target temperatures for fuel performance during irradiation.

2.1 Alloying and Casting

Samples were alloyed via arc-melting in a copper hearth. Following the initial melting of the alloy constituents, the formed button (10-15g) was flipped and re-melted a minimum of 2 times to produce an even mixing. U-xMo-ySi and U-4Si ingots were drop-cast via arc-melting into a 5 mm split copper hearth. U-Nb-Zr ingots were either drop-cast via vacuum-assisted arc melting into 4 mm diameter pins in a copper hearth for heat treatment and property testing or drop-cast into a 6.25 mm copper hearth for interactions testing. Zirconium chunks were arc-melted and drop cast into a 9.5 mm diameter rod used for interactions testing. The arc-melting system and sample pins and hearths are pictured in Figures 1 and 2. Sample identifiers with constituent weights are provided in Table 1 for pins used for heat-treatment and material property testing and Table 2 for material interactions testing.

Figure 1. Arc-melter with button and split hearths.

Figure 2. 4 mm diameter pin of U-Nb-Zr.

Table 1. Alloy information for pins cast for homogenization testing.

Pin ID	Nominal Composition	**dU (g)**	**Nb (g)**	**Zr (g)**
		Mass (g)	**Mass (g)**	**Mass (g)**
1974-1	U-43.28Nb-14.65Zr	4.240	4.364	1.475
1974-2	U-43.28Nb-14.65Zr	4.394	4.517	1.513
2071-1	U-43.28Nb-14.65Zr	4.054	4.172	1.417
2071-2	U-43.28Nb-14.65Zr	4.297	4.410	1.493
		dU	**Mo (g)**	**Si (g)**
2073-1	U-1Mo-2Si	14.564	0.154	0.307
2073-2	U-1Mo-2Si	14.551	0.154	0.300
2073-4	U-1Mo-2Si	14.528	0.152	0.299
2119-1	U-2Mo-1Si	14.843	0.308	0.153
2119-2	U-2Mo-1Si	14.504	0.298	0.149
2119-3	U-2Mo-1Si	14.892	0.309	0.154
2119-4	U-2Mo-1Si	14.467	0.145	0.290
1840	U-4Si	35.40	-	1.398

Table 2. Alloy information for pins cast for material interactions testing.

Pin ID	Nominal Composition	**dU (g)**	**Nb (g)**	**Zr (g)**
		Mass (g)	**Mass (g)**	**Mass (g)**
2071-3	U-43.28Nb-14.65Zr	8.822	9.076	3.075
1997-3	U-43.28Nb-14.65Zr	37.294	38.373	12.989
		dU	**Mo (g)**	**Si (g)**
2072-1	U-1Mo-2Si	13.048	1.440	-
2073-1	U-1Mo-2Si	14.564	0.154	0.307
2119-4	U-2Mo-1Si	14.467	0.145	0.290

2.2 Heat-Treatment Testing for Homogenization

U-Nb-Zr samples were heat-treated in a graphite furnace under high vacuum ($<1x10^{-3}$ mbar) according to tests conditions described in Table 3. Samples (x2 per test) were wrapped individually in Ta or Zr foil and placed in an alumina crucible, pictured in Figure 3. Samples were allowed to cool in the furnace, then prepared for characterization via scanning electron microscopy (SEM) or X-ray diffraction (XRD).

Figure 3. Heat-treatment samples wrapped in foil in alumina crucible.

Table 3. Test summary for homogenization of U-Nb-Zr.

ID	Bake out time at 200°C (hours)	Target Temp (C) (ramp 20°C/min)	Hold at Target temp (hours)	foil
1974-1A	10	900	48	Ta
1974-1B	2	1200	48	Ta
1974-1D	2	1500	48	Zr

U-1Mo-2Si samples (2073-4A, 2073-4C) were heat-treated using a similar method as the U-Nb-Zr samples, with conditions shown in Table 4. Sample 4C was sealed into a quartz ampoule at approximately $1x10^{-5}$ mbar and heated to 700°C for 4 hours. It was then quenched in water by breaking the ampoule. U-2Mo-1Si samples were individually wrapped in Ta and sealed in a quartz ampoule under high vacuum, as pictured in Figure 4. Samples were heated and cooled according to Table 4.

Figure 4. Heat-treatment samples wrapped in foil, sealed in quartz ampoules, and placed inside furnace.

Table 4. Test summary for homogenization of U-1Mo-2Si and U-2Mo-1Si.

ID	Bake out time at 200°C (hours)	Target Temp (°C) (ramp 20°C/min)	Hold at Target temp (hours)	Cooling
2073-4A	2	900	48	Natural
2073-4B	2	700	48	Natural
2073-4C	n/a	700	48	Water quench
2119-3A	n/a	700	48	Natural
2119-3B	n/a	700	48	Water quench
2119-3C	n/a	900	48	Natural

Samples were characterized via backscattered electron detection (BSE) and energy dispersive spectroscopy (EDS) using a JOEL IT-500-HR SEM. EDS maps, line scans, and quantitative point identification were generated using Oxford Intstruments Aztec software. Prior to SEM analysis, samples were metmounted in epoxy, polished to 1um using diamond suspension, and sputter coated with gold.

Samples characterized via XRD (Aeris Malver-Panalytical) were mounted in Crystalbond, polished to 1um, then removed from Crystalbond using acetone.

2.3 Thermal Property and Hardness Testing

Thermal property testing was performed on as-cast material following sample cutting. Samples were sectioned and ground via 600 grit SiC grinding paper to ensure flat, parallel surfaces as needed. Measurements performed to collect data for thermal conductivity were conducted on two different instruments. A Netzsch Differential Scanning Calorimeter (DSC404) was used to collect specific heat capacity data, and a Netzsch laser flash analyzer (LFA427) was used to collect thermal diffusivity data. All measurements were conducted under ultra-high purity Argon that was passed through an Oxy-Gon 120M getter furnace. Data was collected on replicates of material from room temperature to 1200°C at 10°C/min for specific heat, and 5°C/min between isothermal steps for thermal diffusivity.

Specific heat capacity data was collected using a DSC instrument according to the procedure outlined in ASTM E1269-11. The instrument baseline was determined with empty crucibles from Pt/Rh with Yttria lining. These same crucibles were used for all measurements of the same sample set. A sapphire reference was used as a calibration and verification of the data. Values for this test were within 2% of literature values for the specific heat of sapphire. The specific heat of the U-Nb-Zr samples was calculated from the DSC curve for the specimen using the methodology described in ASTM E1269-11.

Thermal diffusivity was measured using a pulse laser flash analyzer based upon the ASTM E1491-13. This measurement method is an isothermal test where data is collected after the specimen comes to thermal equilibrium at a programed temperature. Each sample was measured from room temperature to 1200°C with data being collected approximately every 100°C. Five shot curves were collected at each temperature step and the average value for these five shots is used for the calculation of thermal conductivity. An Inconel 600 standard reference material was used to validate the operation of the LFA and these data were within ± 3% of literature values.

Vickers hardness testing was performed on U-Nb-Zr as-cast (1997-3) and heat-treated (1200°C for 48 hours, 1974-1B) samples using a LECO LM-248AT micro-indenter with AMH43 software. Samples were mounted in epoxy and polished to 1 um. This was performed using a grid of 12 indentions on two areas of the sample. The hardness value at a point is then determined from the mean length of each indention. Results were averaged and presented individually to show the distribution of the measurements for each sample.

2.4 Material Interactions Testing

Samples were cut from pins cast as described in Section 1.1.1 using an abrasive wafering blade for diffusion couple testing (2-3 mm long). Samples were mounted in Crystalbond, polished on one surface to 1 um, then removed from Crystalbond using acetone. Samples were immediately assembled into kovar diffusion couple jigs with a set screw to ensure contact, as shown in Figures 5 and 6. A thick piece of Ta foil (0.25 mm) was used to isolate the diffusion couples from the kovar and act as an oxygen getter. The assembled jigs were sealed in a quartz ampoule at approximately $1x10^{-5}$ mbar, pictured in Figures 7 and 8. Diffusion couples were then heated for 1 week according to the test matrix shown in Table 5, and allowed to cool slowly inside of the furnace.

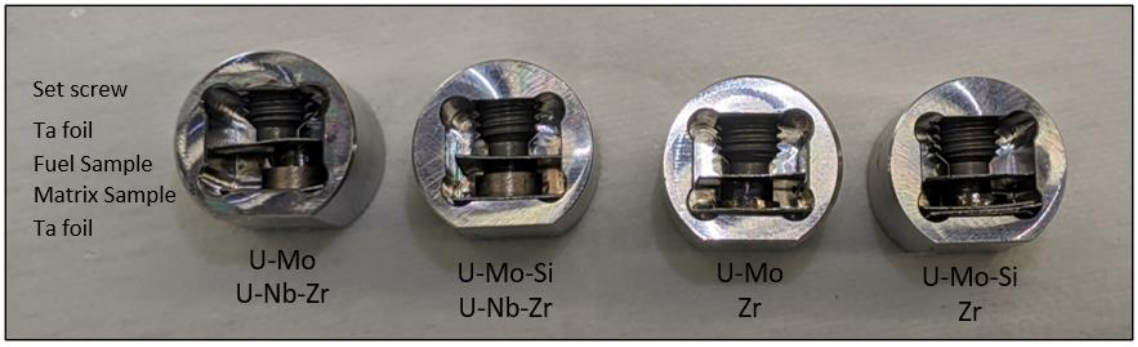

Figure 5. Stack up of diffusion couple assemblies for interaction testing.

Figure 6. Diffusion couple assemblies for interaction testing.

Figure 7. Diffusion couple assemblies sealed in quartz ampoule under high vacuum.

Figure 8. Diffusion couple assemblies sealed in quartz ampoule under high vacuum.

Table 5. Test summary for material interactions.

Fuel	Matrix	Temperature (°C)
U-10Mo (2072-1-1)	U-Nb-Zr (2071-3-1)	700
U-10Mo (2072-1-3)	Zr	700
U-1Mo-2Si (2073-1-1)	U-Nb-Zr (2071-3-2)	700
U-1Mo-2Si (2073-1-3)	Zr	700
U-2Mo-1Si (2119-4-1-3)	U-Nb-Zr (1997-3C-1-A)	700
U-2Mo-1Si (2119-4-1-1)	Zr	700
U-10Mo (2072-1-2)	U-Nb-Zr (2071-3-3)	600
U-10Mo (2072-1-3)	Zr	600
U-1Mo-2Si (2073-1-2)	U-Nb-Zr (2071-3-4)	600
U-1Mo-2Si (2073-1-4)	Zr	600
U-2Mo-1Si (2119-4-1-4)	U-Nb-Zr (1997-3C-1-B)	600
U-2Mo-1Si (2119-4-1-2)	Zr	600

Following heating, diffusion couples were removed from the ampoule but not removed from the jig to maintain the applied pressure. The diffusion couple assembly was then mounted in epoxy and the excess length of the jig was cut off using an abrasive wafering blade without cutting into the diffusion couple samples. The diffusion couples were then ground to the approximate mid-plane using SiC grinding paper to analyze the maximum length of the diffusion layer. The interface was then polished to 1 um, gold-coated, and analyzed on SEM using BSE and EDS. Due to overlap of the L-series EDS peaks in Nb and Mo, the EDS map and line scan were performed using a single peak for identification of Mo, as shown in Figure 9, in diffusion couples containing U-Nb-Zr.

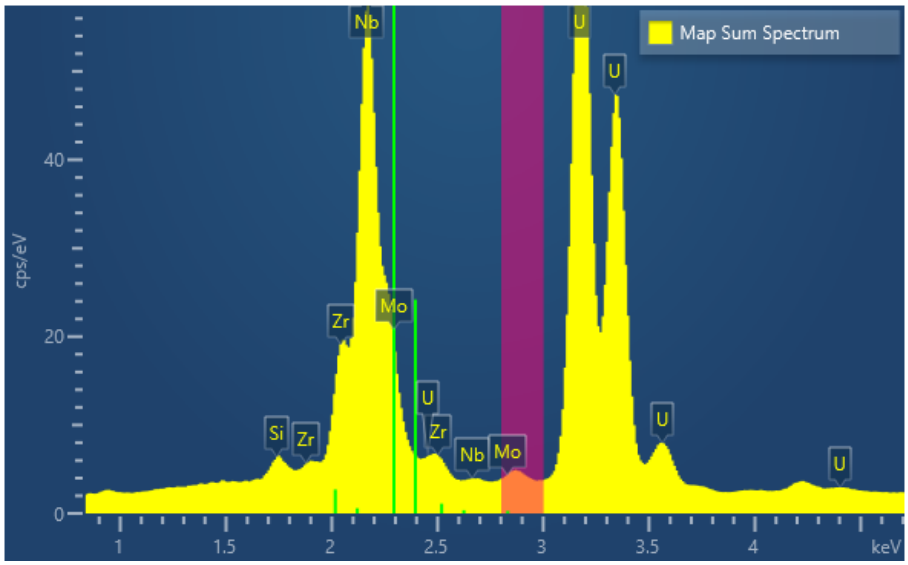

Figure 9. EDS spectrum showing peak overlap in Nb and Mo; Mo L-series indicated by green lines and identification peak used highlighted in pink region.

3. RESULTS

3.1 Advanced Fuel Candidate Characterization

3.1.1 U-4Si Microstructural Characterization

The initial as-cast material of U-4Si (ID 1840) was analyzed via SEM imaging. The low magnification image, shown in Figure 10a, shows two distinct regions that were suspected to be a Si-rich structure distributed in a U-rich matrix. However, upon examination at higher magnification, shown in Figure 11, the matrix consists of smaller regions with varying composition. The EDS map and point analysis confirms that the concentration of Si dispersed through the uranium varies significantly. It was suspected that the inhomogeneous composition was due to insufficient mixing during casting, so the alloy was re-cast 5 times, with samples taken from each casting. Figure 10 shows the BSE images from the first (Figure 10b) and final (Figure 10c) recast alloy. The red boxes shown in Figure 10 represent areas evaluated more thoroughly in Figures 11-13.

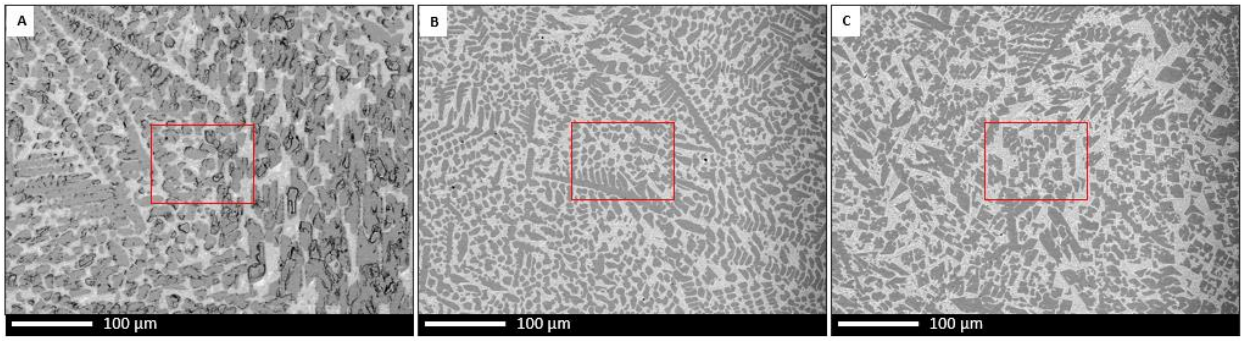

Figure 10. Low magnification BSE images of U-4Si as-cast samples after (from left to right) initial casting (A), first re-casting (B), and fifth re-cast (C).

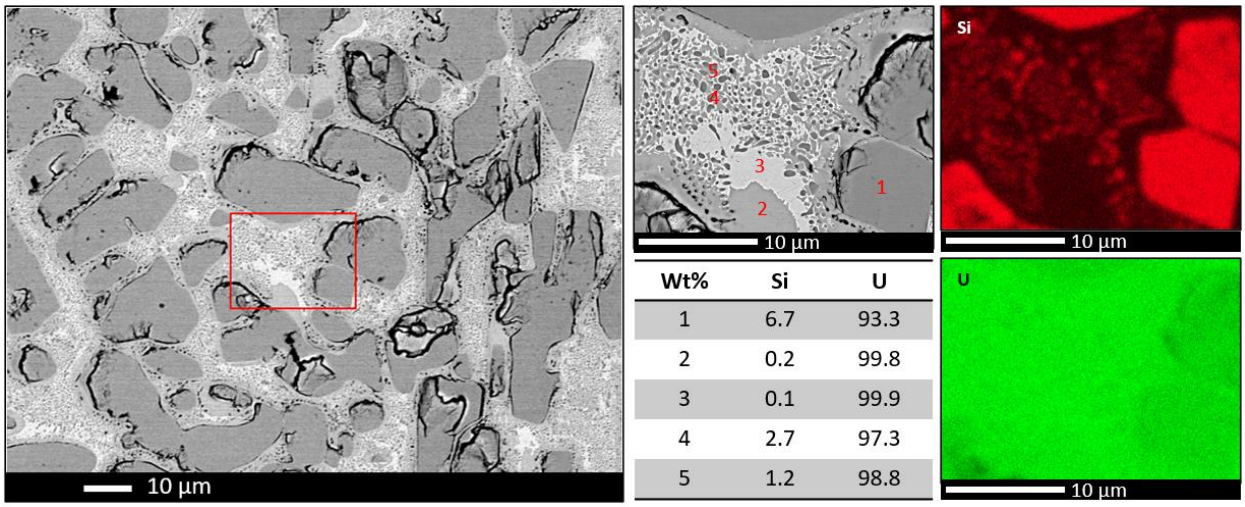

Wt%	Si	U
1	6.7	93.3
2	0.2	99.8
3	0.1	99.9
4	2.7	97.3
5	1.2	98.8

Figure 11. High magnification BSE images and EDS maps and point identification of initial as-cast sample from Figure 10a.

The re-cast samples consisted of a similar microstructure as the initial casting, with Si-rich structures dispersed throughout the samples. The U-rich matrix also contained a secondary structure with more discreet segregation of the Si and U within the matrix. The increased number of melting/casting attempts also affected the morphology of the microstructure. The small Si-rich inclusions within the U-rich phase became larger and less abundant after the additional casting attempts. The larger Si-rich structures also became more angular. This may be an indication of differences in cooling rates between the samples. If insufficient time was permitted for the hearth to cool between casting attempts, the additional heat retention of the hearth may cause pins from subsequent castings to cool slower. Due to the variety of phases observed in the as-cast material, and complexity of the phases in the U-Si system [6], this alloy was not further investigated.

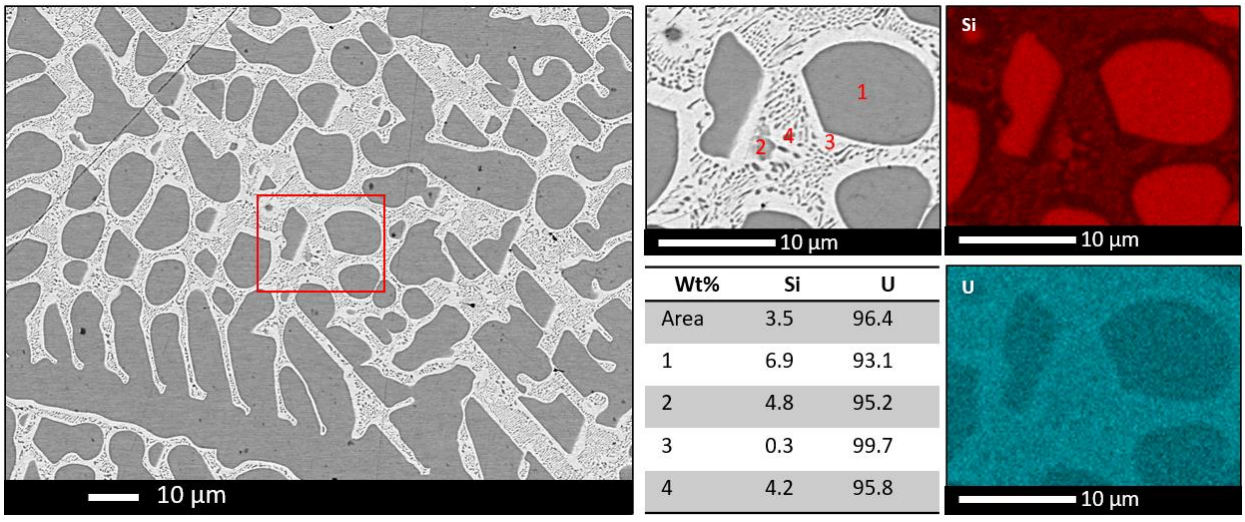

Wt%	Si	U
Area	3.5	96.4
1	6.9	93.1
2	4.8	95.2
3	0.3	99.7
4	4.2	95.8

Figure 12. High magnification BSE images and EDS maps and point identification of the first re-cast sample from Figure 10b.

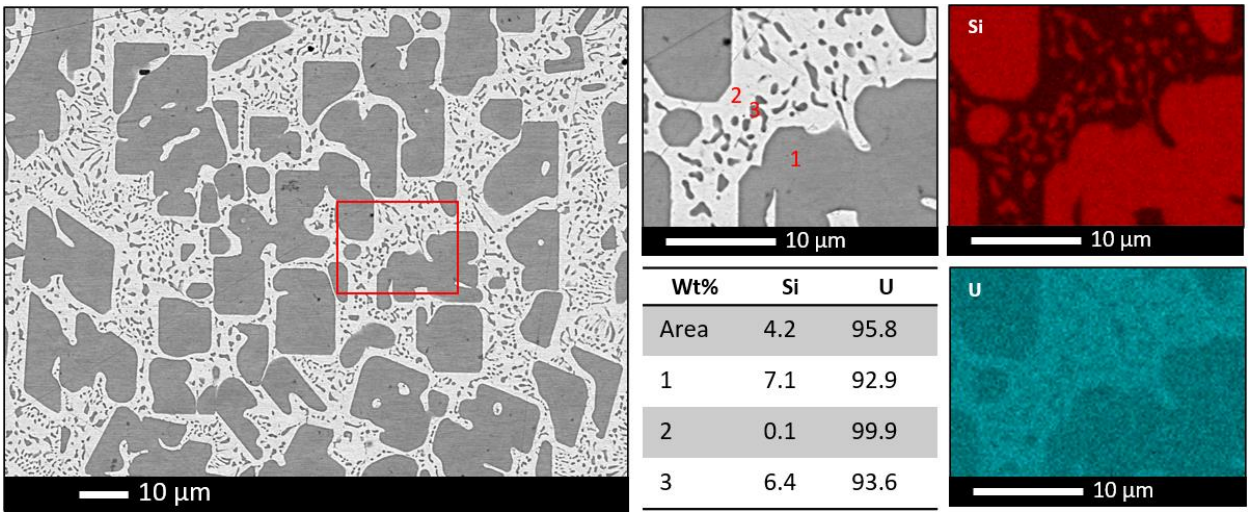

Wt%	Si	U
Area	4.2	95.8
1	7.1	92.9
2	0.1	99.9
3	6.4	93.6

Figure 13. High magnification BSE images and EDS maps and point identification of the fifth re-cast sample from Figure 10c.

3.1.2 U-1Mo-2Si Microstructural Characterization

The samples of U-1Mo-2Si following heat treatment tests are shown in Figure 14. The first test at 900°C resulted in a significant deformation and oxidation of the sample. This may have been caused by localized melting in a non-homogeneous sample, so the subsequent tests were performed at a lower temperature. The sample heated at 700°C still showed significant surface oxidation, but maintained its structural integrity, supporting the theory that localized melting did occur at 900°C. After surface oxidation was observed from samples heated within the high vacuum furnace, samples for subsequent tests were sealed in a quartz ampoule under high vacuum. No surface oxidation was visually observed on the sample quenched from 700°C, confirming that the sealed quartz ampoule produced a better atmosphere than the furnace alone.

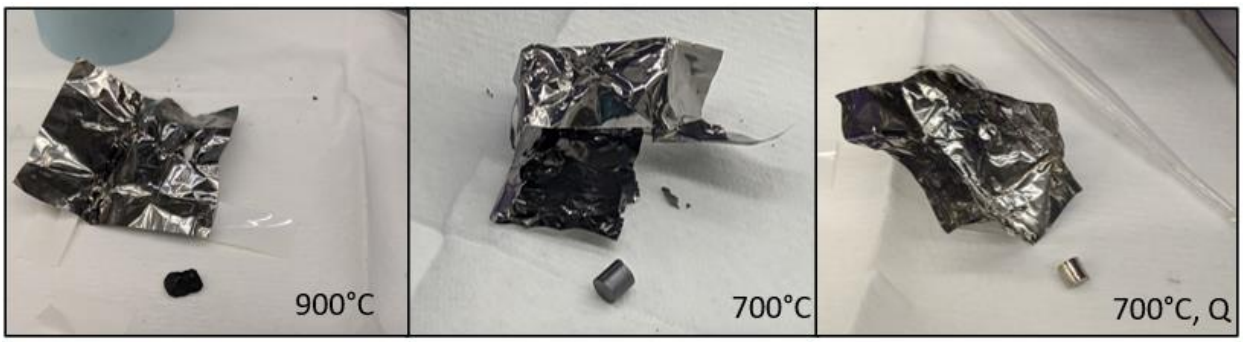

Figure 14. U-1Mo-2Si after heating to 900°C, 700°C

Each of the samples were imaged at a consistent low magnification in order to compare the resulting microstructure, as shown in Figure 15. The as-cast microstructure varied significantly from the center of the sample and the edge. The microstructure of the convection-cooled 700°C

sample was consistent throughout the observed surface. The remaining tests (900°C, quenched 700°C) contained regions with significant variation. A significantly different microstructure was observed in each sample, and the regions indicated in a red box were analyzed in more detail.

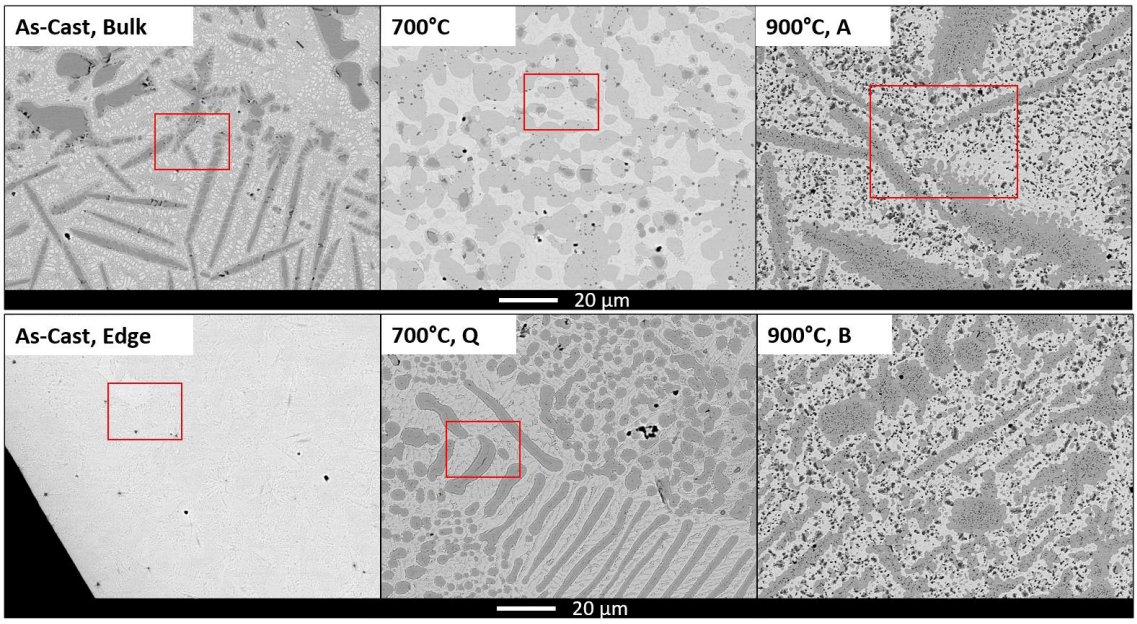

Figure 15. Comparison of U-1Mo-2Si as-cast and heat-treated samples via BSE imaging.

High-magnification EDS maps taken at the center of the as-cast sample, Figure 16, show Si-rich dendrites dispersed in a U-rich matrix. The matrix itself also consisted of regions containing higher concentrations of either Mo or Si. These variations, though qualitatively observed, appear minor compared to the difference between precipitate and matrix. The morphology at the edge of this sample is a more homogeneous mixture of U, Mo, and Si, shown in Figure 17, with an area-averaged composition closer to the target nominal composition of the alloy. This could be caused by the relative difference in cooling rates between the center and the edge of the sample during the casting process. Since the edge of the sample is in contact with the water-cooled copper hearth, it could cool at a faster rate than the center of the rod. This faster cooling may prevent the various phases from forming while cooling.

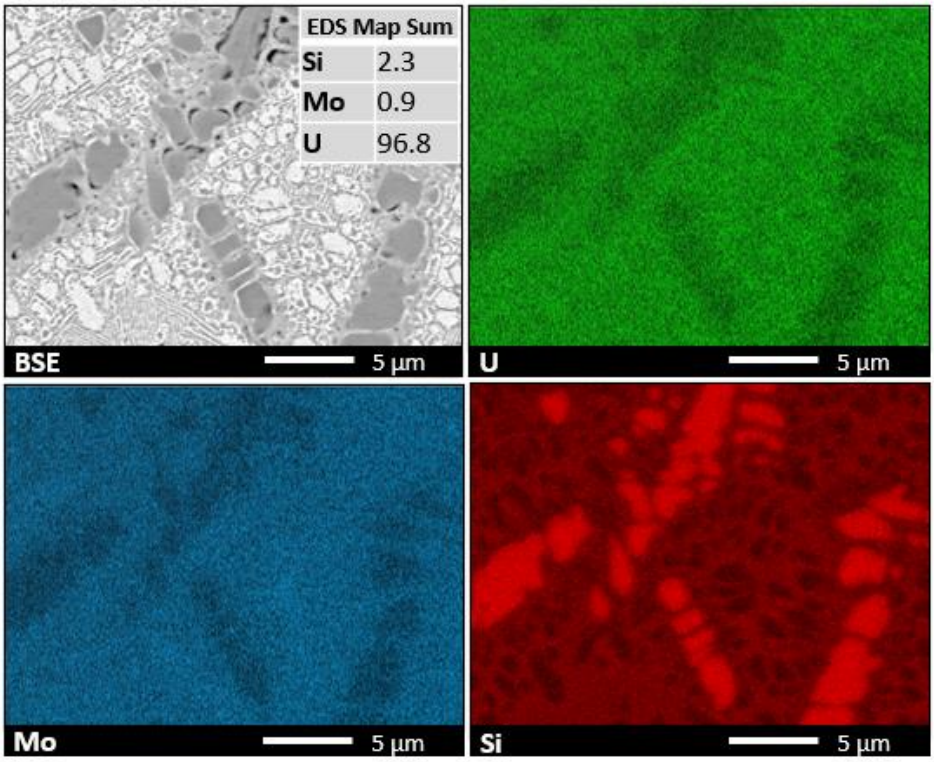

Figure 16. EDS maps of U-1Mo-2Si bulk as-cast microstructure.

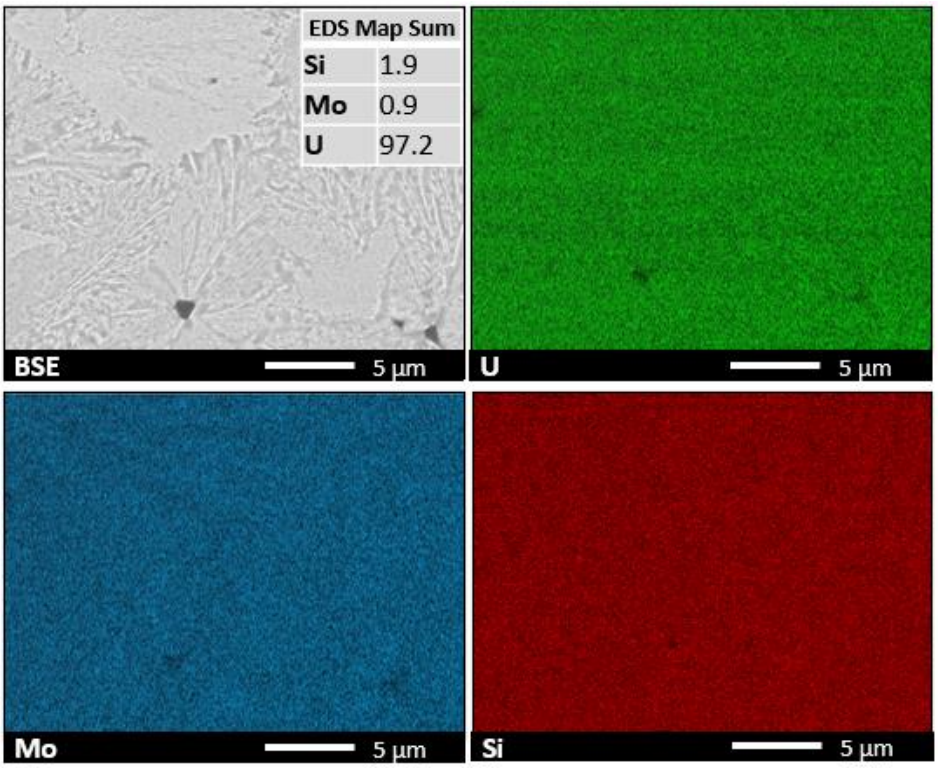

Figure 17. EDS maps of U-1Mo-2Si as-cast microstructure at the edge of the sample.

The sample heated to 700°C appeared to have a more distinct separation of phases than the as-cast sample. U-Si features, such as that indicated as 'A' in Figure 18, can be observed in the EDS maps, as well as Mo and Si rich features (B). The U-rich bulk structure (C) appeared more homogeneous in the BSE images, however the EDS maps showed a separation of U and Mo, causing Mo-rich intragranular features (D) to form along grain boundaries in the U-rich phase. The re-structuring of phases observed in this sample compared to the as-cast sample suggested the temperature was sufficiently high to initiate the breakdown and reforming of phases, though the slow cooling rate allowed other phases to reform. water the effects of rapid cooling on the microstructure, with the goal of reproducing a similar structure as observed in the edge of the as-cast sample. The quenched sample, however, showed similar restructuring as the slow cooled sample, shown in Figure 19. It exhibited more variation in the arrangement of the distinct phases, such as the (Mo-Si)-rich phase within U-Mo-Si phase rather than the spots around the U-Mo-Si.

The phases in the sample heated to 900°C appear even more segregated than in the 700°C samples, shown in Figure 20. A U-Mo-Si phase can be observed within the U-Si structures. Small, but abundant, areas consisting of a (Mo-Si)-rich phase also appears dispersed throughout, showing Mo favoring Si over U. Since ternary phase diagrams for this system are not well developed at temperatures above 850°C, additional phases could be forming at these elevated temperatures [7].

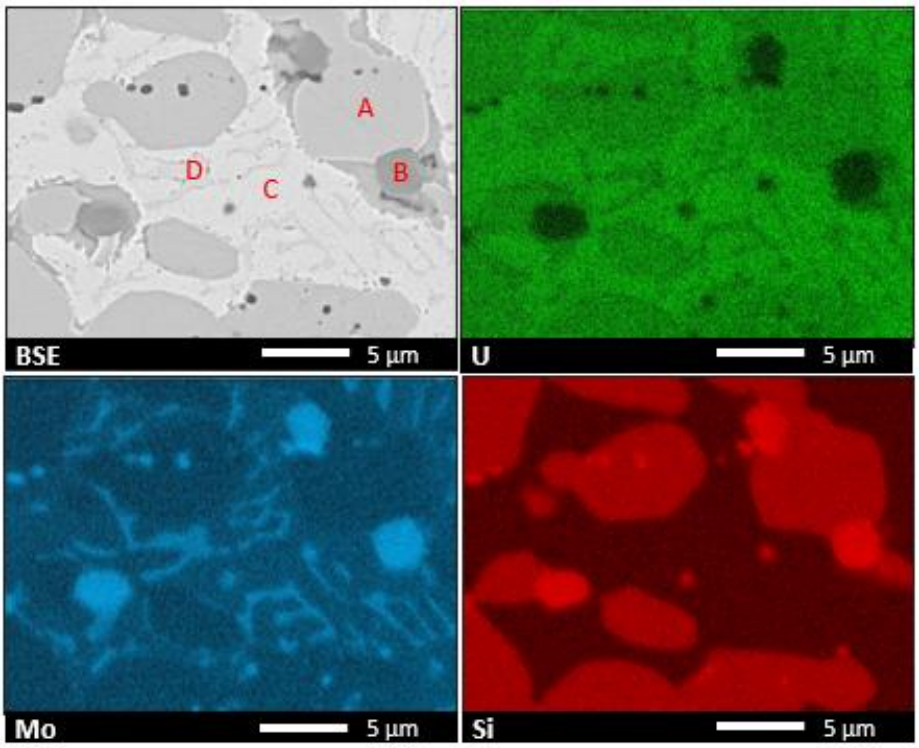

Figure 18. EDS maps of U-1Mo-2Si (700°C) microstructure.

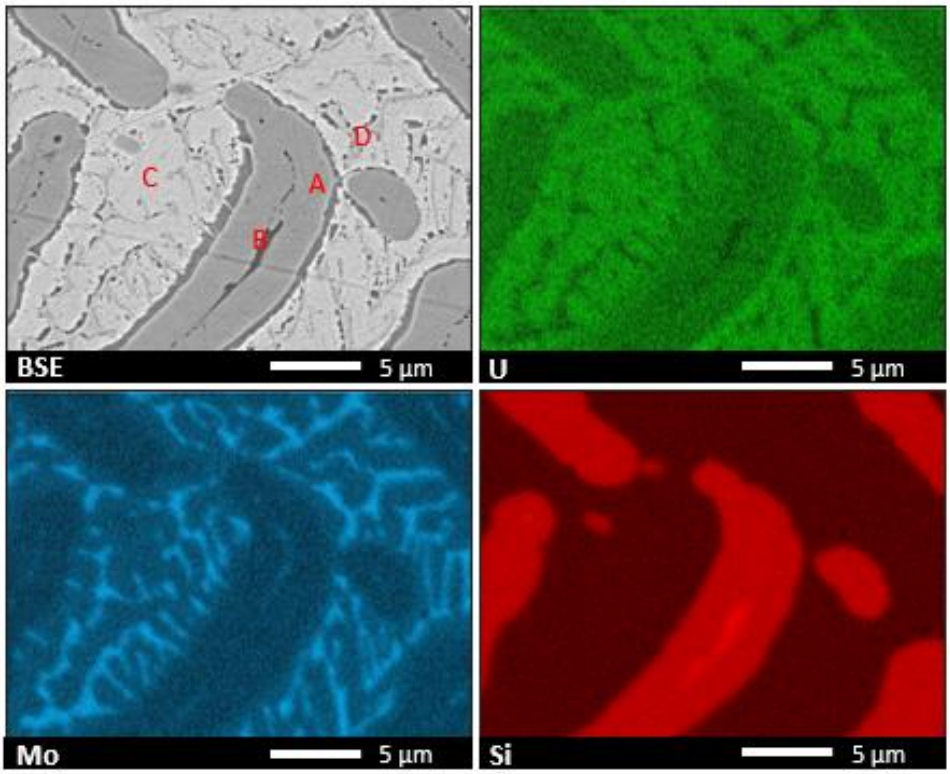

Figure 19. EDS maps of U-1Mo-2Si (700°C, quenched) microstructure.

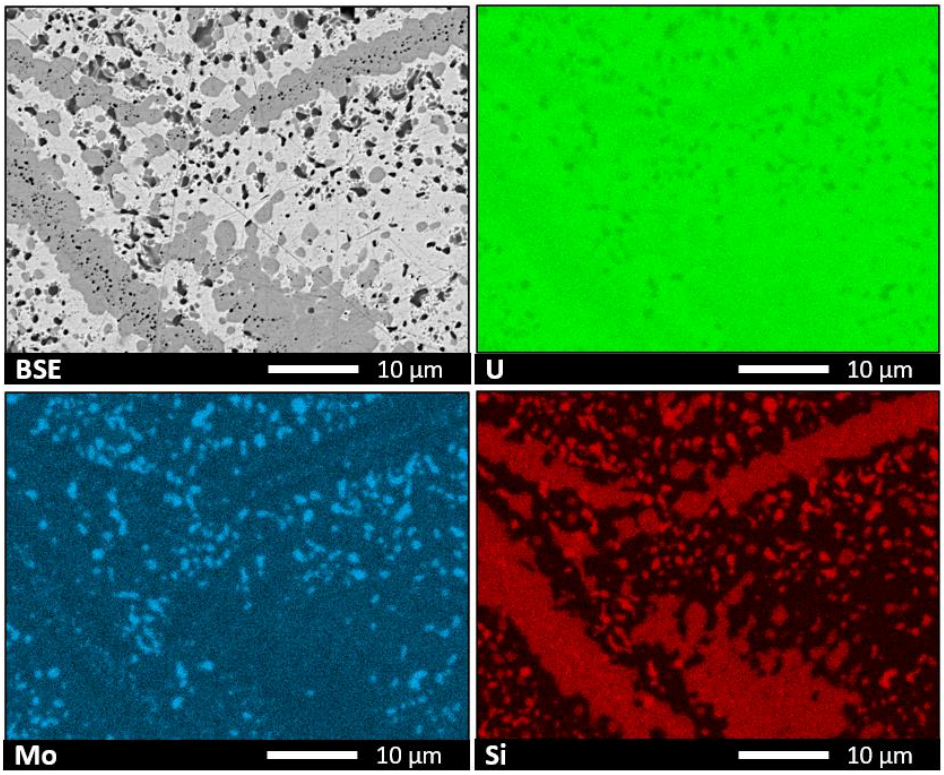

Figure 20. EDS maps of U-1Mo-2Si (900°C) microstructure.

3.1.3 U-2Mo-1Si Microstructural Characterization

Each of the U-2Mo-1Si samples were imaged via BSE at a consistent low magnification in order to compare the resulting microstructures, as shown in Figure 21. The morphology of each of the samples was consistent across its surface but consisted of some slight local variations in the arrangement of phases, particularly in the as-cast sample. A significantly different microstructure was observed in samples heat treated at different temperatures, and the regions indicated in a red box were analyzed in more detail and shown in Figures 22-26.

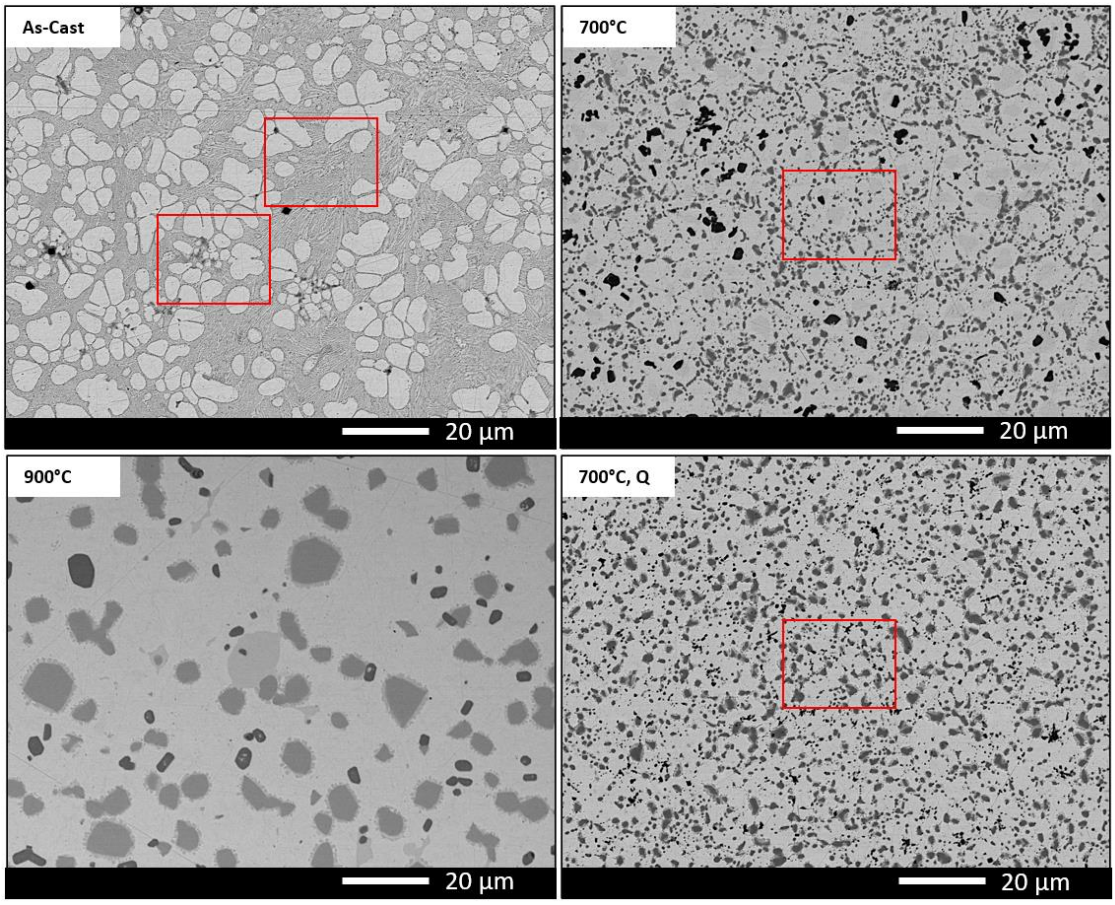

Figure 21. Comparison of U-2Mo-1Si as-cast and heat-treated samples via BSE imaging.

The as-cast microstructure consisted of two main regions, a U-Mo-Si matrix clusters of U-Mo precipitates, as shown in Figure 22. According to the EDS point identifications, The U-Mo cluster were consistently a composition of approximately U-2wt%Mo. The matrix exhibited a secondary lamella microstructure, which can be observed in the BSE image and EDS map of region A in Figure 22. The lamella structure appears to be based on differences in the Si concentration, with some variations in the Mo concentration throughout. The middle of the U-Mo clusters also has areas with variations in compositions, which can be observed from the EDS point identifications and maps in Region B of Figure 22. Figure 23 shows a high magnification BSE image with EDS maps of region observed in the as-cast sample. This region presents similar phase compositions, but with a different arrangement of the features.

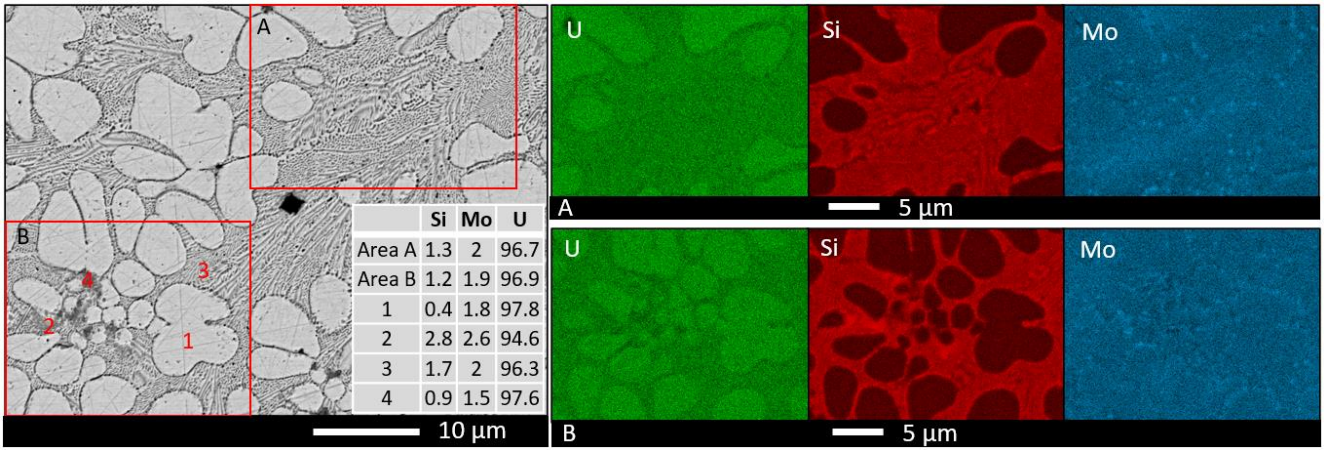

	Si	Mo	U
Area A	1.3	2	96.7
Area B	1.2	1.9	96.9
1	0.4	1.8	97.8
2	2.8	2.6	94.6
3	1.7	2	96.3
4	0.9	1.5	97.6

Figure 22. Low magnification EDS maps and point identification of U-2Mo-1Si as-cast microstructure.

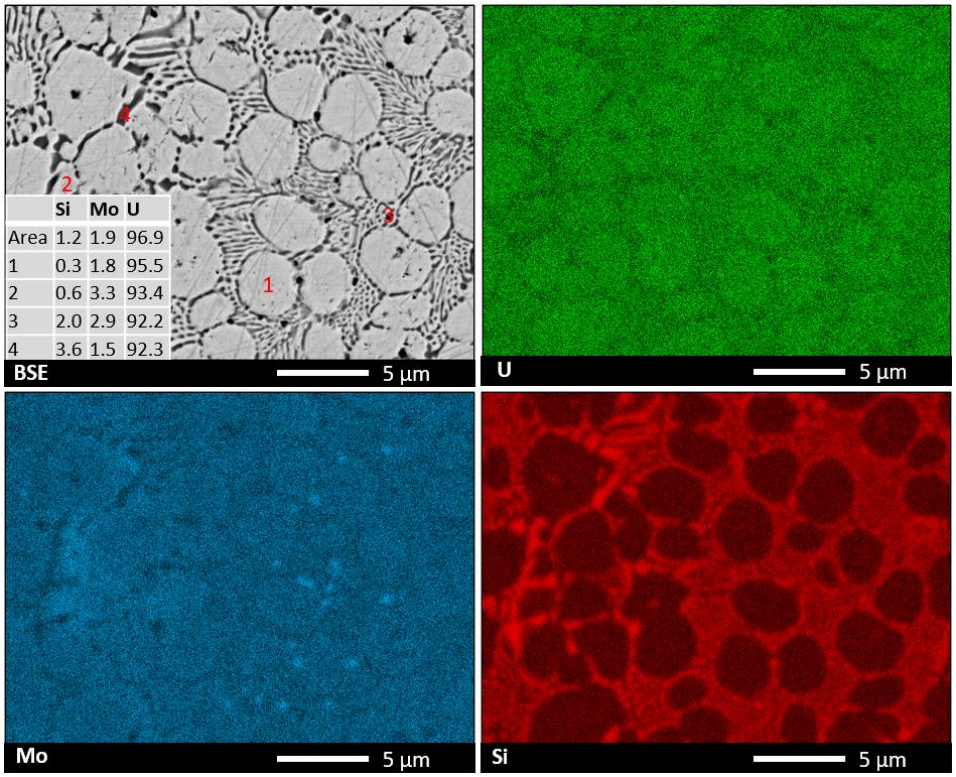

	Si	Mo	U
Area	1.2	1.9	96.9
1	0.3	1.8	95.5
2	0.6	3.3	93.4
3	2.0	2.9	92.2
4	3.6	1.5	92.3

Figure 23. EDS maps and point identification of U-2Mo-1Si as-cast microstructure.

The quenched and non-quenched samples consist of a similar microstructure, though with more discreet phase segregation in the non-quenched sample, as shown in Figures 24 and 25. This microstructure exhibits a predominate U-rich matrix with precipitates containing higher Mo and Si concentration (5-15 wt% of each) throughout. Within the U-rich matrix, regions with low concentrations (approximately 2 wt%) of Mo were observed. The regions, indicated as points '1' in Fig. 24 and 25, are difficult to distinguish in the BSE images, but are more apparent in the

EDS maps, specifically those of Mo. The secondary lamella structure observed in the as-cast sample was not observed in the heat-treated samples.

The sample heat-treated at 900°C exhibited 3 distinct phases – a U-rich matrix, U-Si precipitates, and U-Mo-Si precipitates with the varying concentrations of Mo and Si, as shown in Figure 26. The intermediate U-Mo phase that was observed in the 700°C sample was not present in this sample.

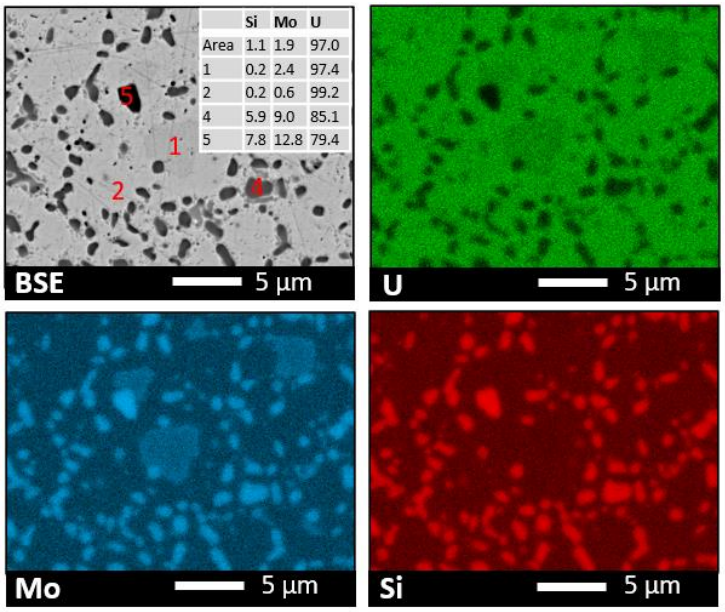

Figure 24. EDS maps and point identification of U-2Mo-1Si (700°C) microstructure.

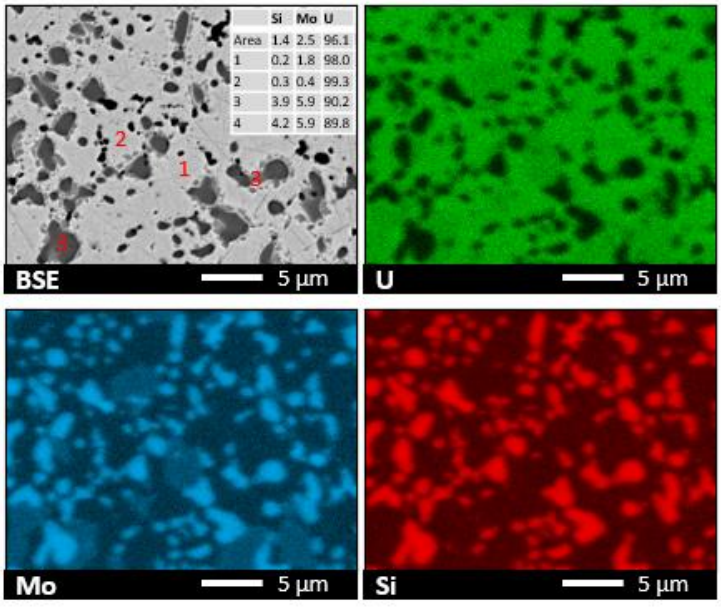

Figure 25. EDS maps and point identification of U-2Mo-1Si (700°C, quenched) microstructure.

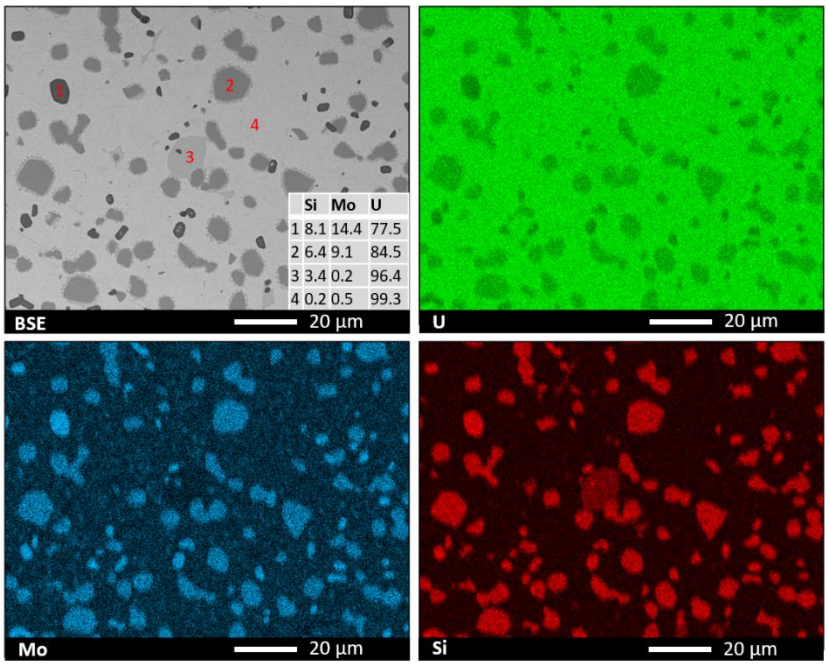

Figure 26. EDS maps and point identification of U-2Mo-1Si (900°C) microstructure.

3.2 Fissile Matrix Candidate (U-43.28Nb-14.65Zr) Characterization

3.2.1 As-cast and Heat-treated Microstructure

The microstructure of the as-cast U-Nb-Zr alloy consisted of Nb-rich dendritic precipitates in a U-rich matrix. The Zr content remained consistent within these two regions, with the concentration only varying by up to 5 wt%. The U and Nb concentration, however, varies by up to 40 wt% between these regions. Some intermediate regions were observed, indicated by points 2 and 3 in Fig. 27, indicating incomplete segregation between the dominate phases.

Initial heat-treatment testing started at 900°C for 48 hours. In Figure 28, it can be observed that the Nb dendrites begin to decompose at this temperature, as the dendrites appear smaller and more variation of the elemental concentrations within the U-rich matrix can be observed in the differences between points 1, 2, and 3.

At 1200°C, the dendritic structures were no longer observed, shown in Figure 29. No observable variations were present within the matrix, with the exception of small Zr precipitates distributed throughout the sample. Although the presence of Zr precipitates is not ideal, this phenomenon is common in U-Zr fuels. EDS analyses were performed on an area containing Zr precipitates. The difference between Zr content for the entire region was within 0.5-1.0 wt% of the concentration within the matrix, suggesting that the precipitates have little impact on the overall composition. Each of the elements within the fuel was analyzed to be within 1.0 wt% of the target composition. These results demonstrate that a solid solution potentially began forming around 900°C and was completely formed by 1200°C.

The heat-treatment at 1500°C did not impact the formation of the Zr precipitates, as they were still observed in the BSE and EDS imaging shown in Figure 30. At this temperature, however, distinguishing features at the grain boundaries could be observed.

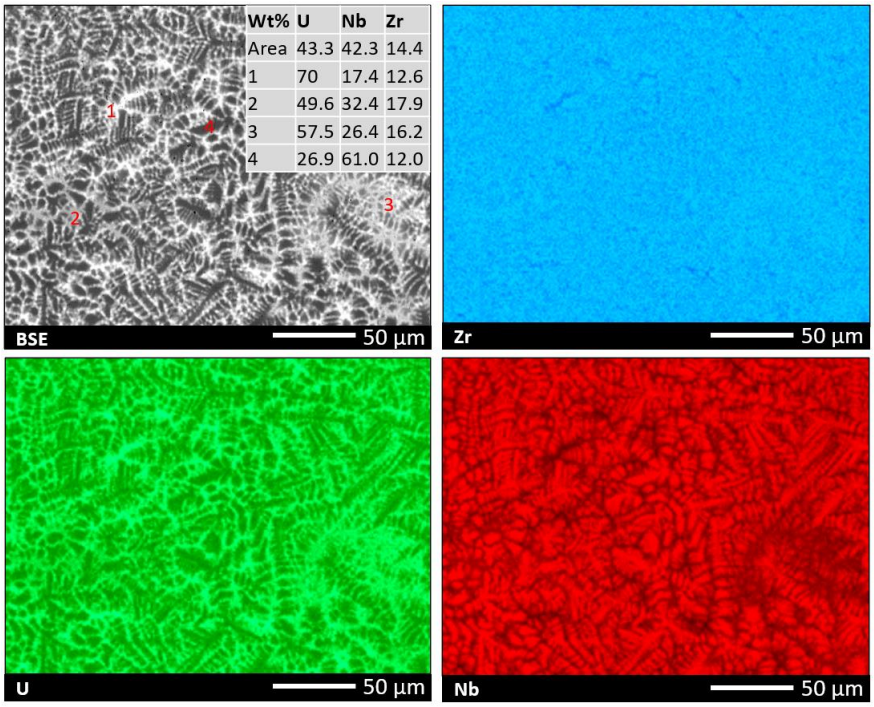

Figure 27. EDS maps and point identification of U-Nb-Zr as-cast microstructure.

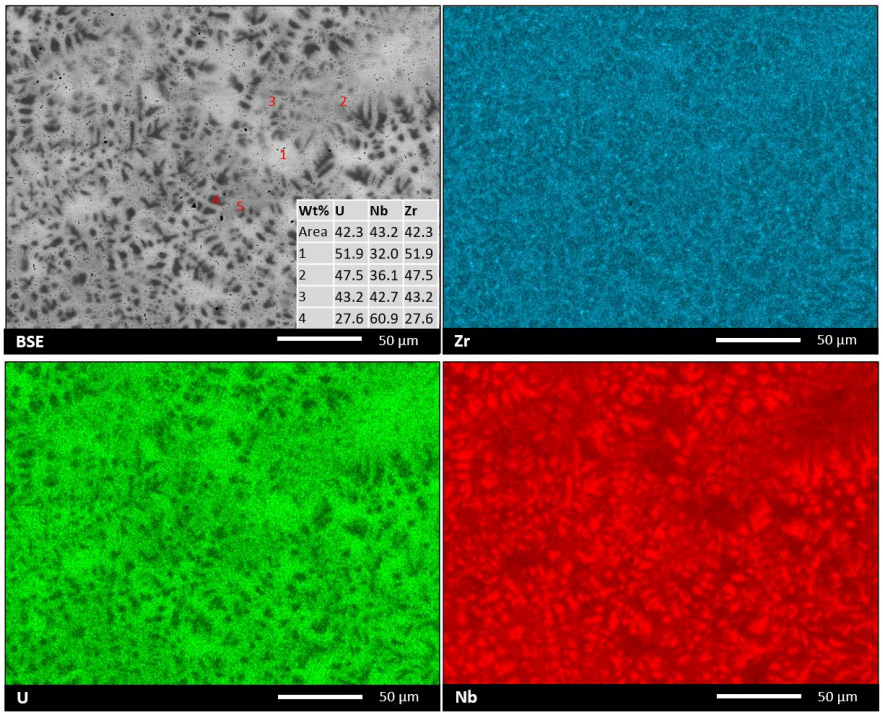

Figure 28. EDS maps and point identification of U-Nb-Zr (900°C, 48 hour) microstructure.

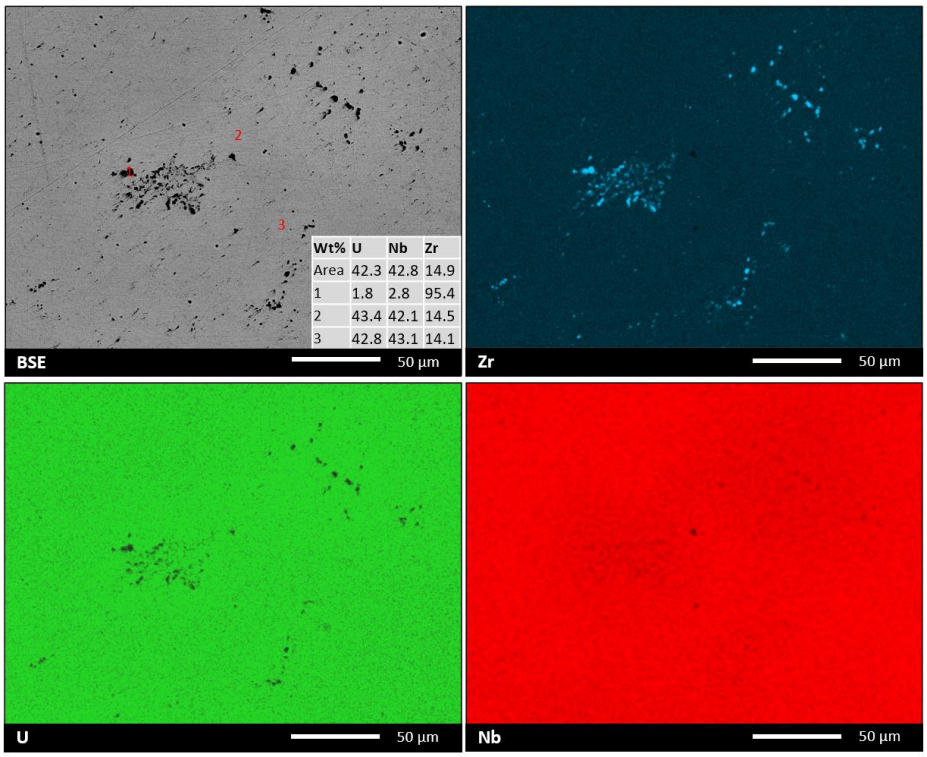

Figure 29. EDS maps and point identification of U-Nb-Zr (1200°C, 48 hour) microstructure.

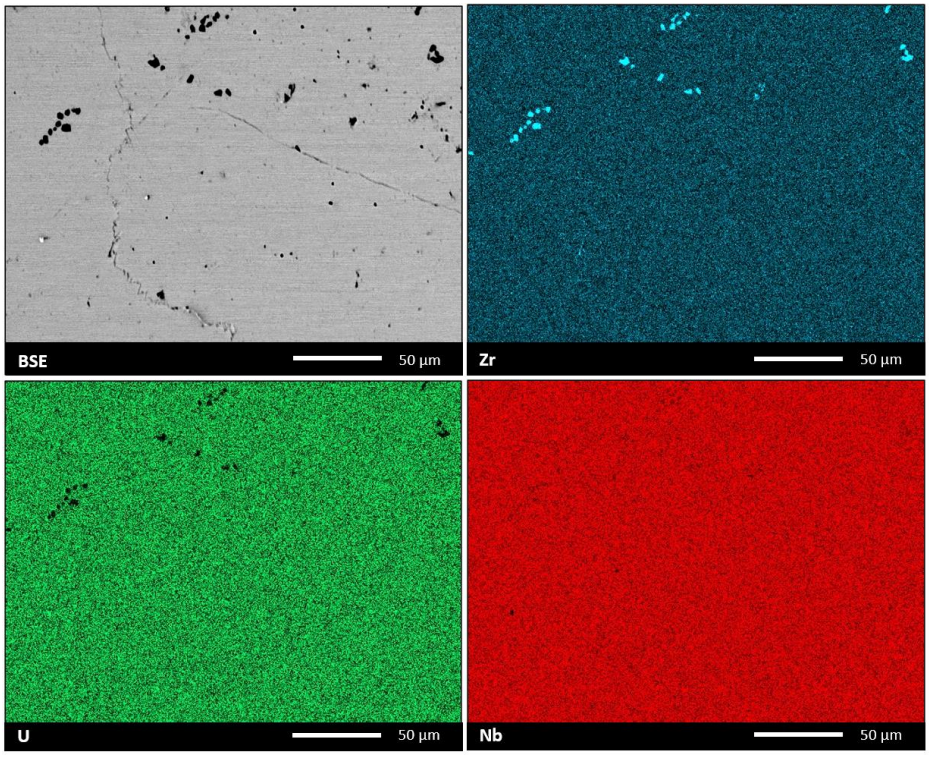

Figure 30. EDS maps and point identification of U-Nb-Zr (1500°C, 48 hour) microstructure.

X-ray Diffraction was performed in the as-cast and heat-treated samples to analyze the crystal structure of the phases formed at the various temperatures. The as-cast sample exhibits BCC peaks, as indexed in Figure 31 [8]. The broadening of the peaks suggests both Nb-rich and U-rich phases that were observed exhibit a BCC structure but may vary enough in lattice parameter to cause a slight peak shift. The overlap between the two BCC phases would then present as a broadened peak, as observed. The sample heated at 900°C exhibits narrower peaks, supporting the analysis from SEM characterization that the two phases begin to decompose at or around 900°C. The spectra for the 1200°C samples consist of sharp BCC peaks, indicating that the presence of the Zr precipitates is below the detection limit of the XRD, and the bulk system presents as a single-phase system. The sample heat-treated at 1500°C contains additional phases as more small peaks can be observed. This temperature was high enough to cause additional restructuring within the sample, which may cause the features at the grain boundaries observed in the BSE images for this sample.

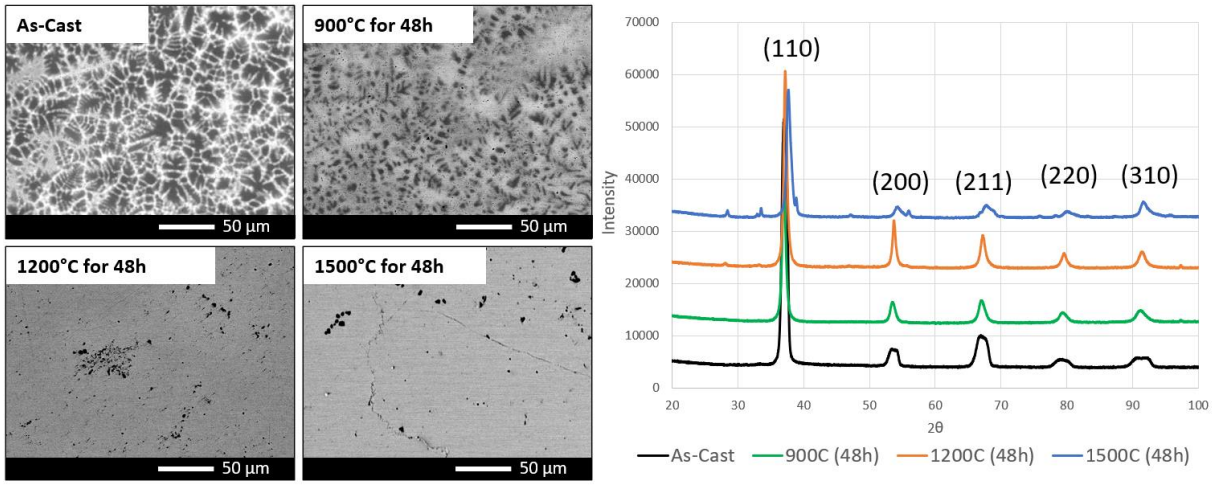

Figure 31. Comparison of as-cast and heat-treated sample microstructure via BSE imaging and XRD.

3.2.2 Thermal Property Testing

Thermal property testing was conducted on the as-cast U-Nb-Zr alloy. Figure 32 shows the DSC signal which identifies phase transitions and is the collected data from which specific heat is calculated. Three heating/cooling cycles were performed on a single sample in the DSC. Notice that Cycle 1 has an exothermic slope in the plot and Cycles 2 and 3 do not. This indicates that upon heating the material immediately began to change its microstructure which is supported by the SEM data above describing the change in the dendritic formations during the heat-treatment study. The heating cycle data also has a small peak at approximately 627 to 649°C and an endothermic (upward) slope at approximately 1045°C. Both of which are not present in the cooling data. This indicates a non-reversible phase change in the material which is again supported by the heat-treatment data. Figure 33 shows the specific heat data upon heating calculated from heat cycles 2 and 3. It is normal exclude the first heating cycle data in further thermal property calculations like specific heat because these data likely represent heats of annealing of the sample material that mask the intrinsic specific heat.

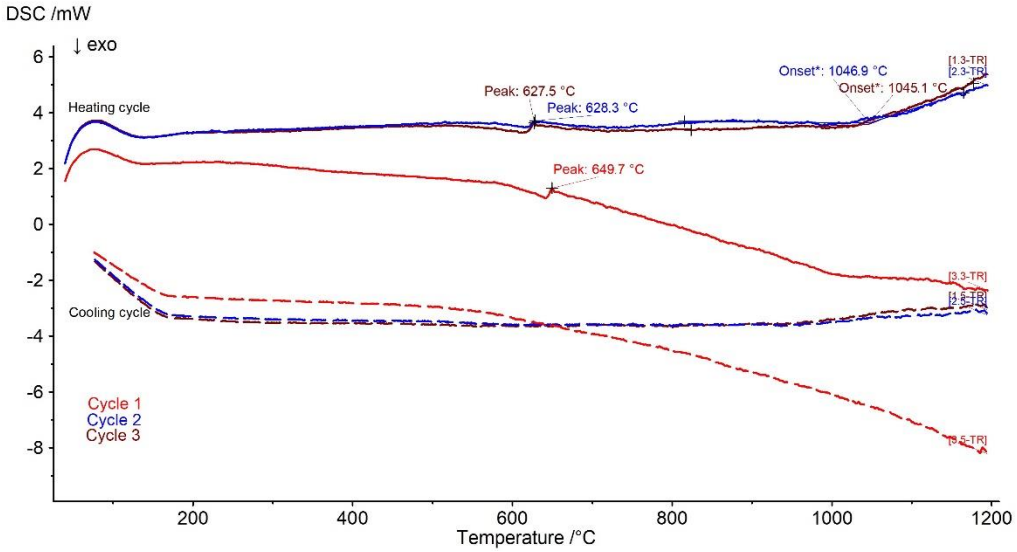

Figure 32. DSC Curve vs. Temperature for U-Nb-Zr alloy upon heating and cooling for 3 cycles.

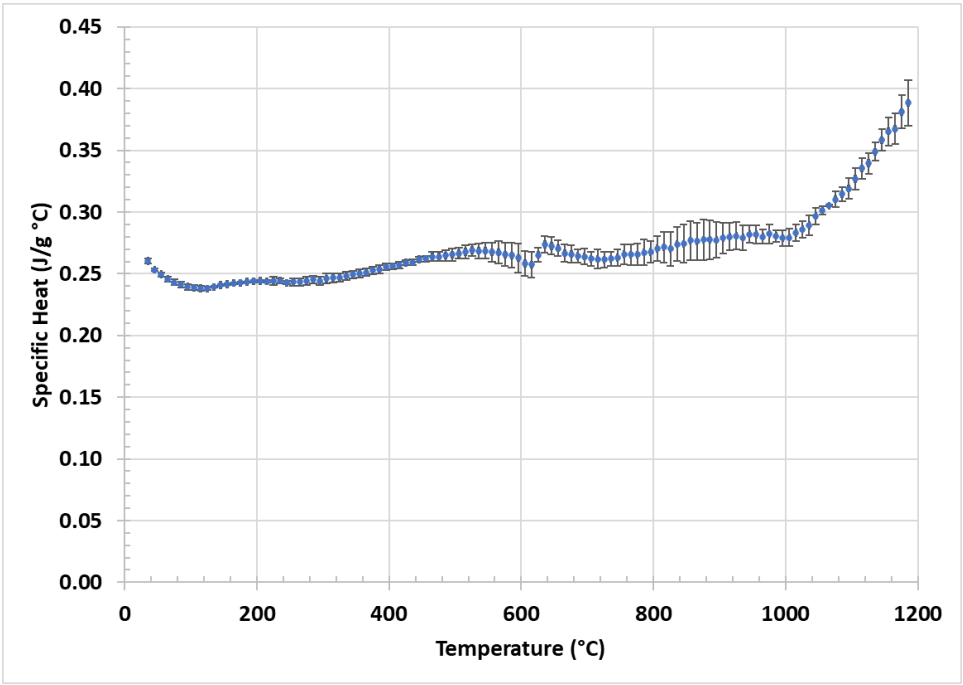

Figure 33. Specific Heat vs. Temperature for U-Nb-Zr upon heating. Averaged data from thermal cycles 3 and 4 with error bars.

Thermal diffusivity was measured using the laser flash analysis method on three separate samples of U-Nb-Zr alloy. Data was collected every approximate 100°C both on heating and cooling and the values were averaged together and are presented in Figure 34. Notice that the values upon heating are higher than those upon cooling and this behavior was consistent between all three samples. This is likely due to the annealing of the material upon heating and that annealing not

being reversible. This is also a reason why the error bars are larger upon heating between the data points collected as well.

Thermal conductivity at room temperature was calculated using the relationship in Equation 1; where k is thermal conductivity, Cp is specific heat at constant pressure, ρ is density, and α is thermal diffusivity.

$$k=Cp\cdot\rho\cdot\alpha \qquad \text{Eq 1}$$

The density value for this U-Nb-Zr alloy was calculated from the mass and volume of the pre-test LFA samples and was determined to be 10.3 g/cm^3. The resulting room temperature thermal conductivity value is 12.3 W/m °C. Future work will include the measurement of thermal expansion over the temperature range in this study. From that thermal expansion data, the density as a function of temperature can be calculated by adjusting the volumetric expansion. Thermal conductivity as a function of temperature will also then be feasible.

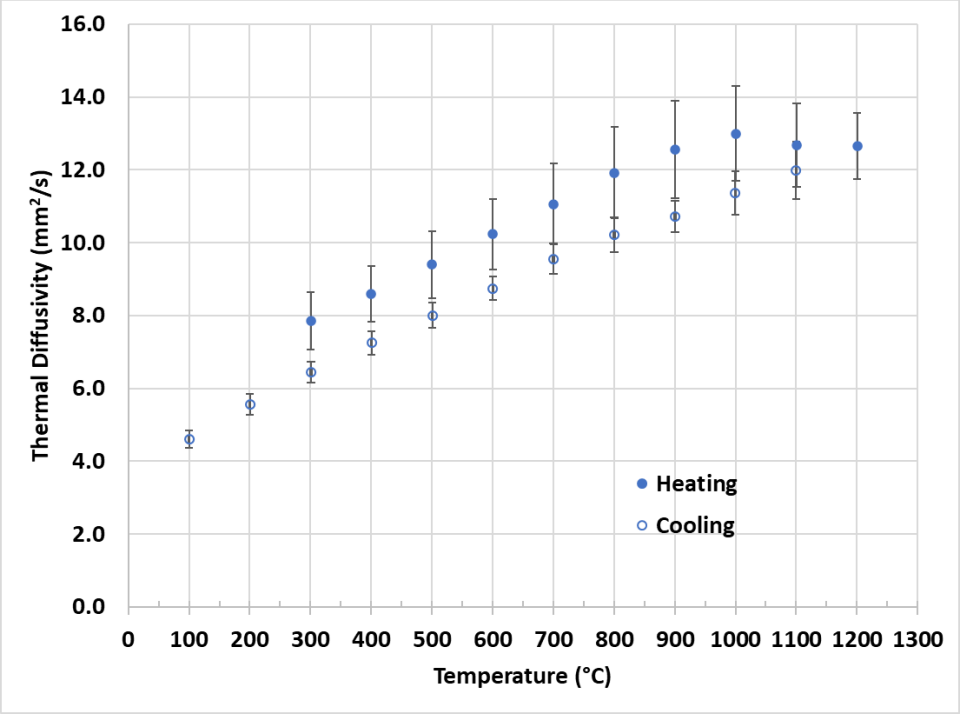

Figure 34. Thermal Diffusivity vs. Temperature for U-Nb-Zr upon heating and cooling. These data are an average of 3 trials of separate specimens.

3.2.3 Micro-hardness Testing

Vickers micro-hardness testing was performed on the as-cast and heat-treated (1200ºC, 48 hours) to compare the mechanical properties of the as-cast and homogenized systems. The indention patterns for the as-cast and heat-treated samples were imaged using an integrated optical microscope and shown in Figures 35 and 36, respectively. The length of each indention was correlated to the hardness value, and the distribution of the resulting Vickers hardness values in shown in Figure 37. Overall, the homogenization heat treatment did not significantly impact the average or range of values but did shift the distribution of the values marginally higher.

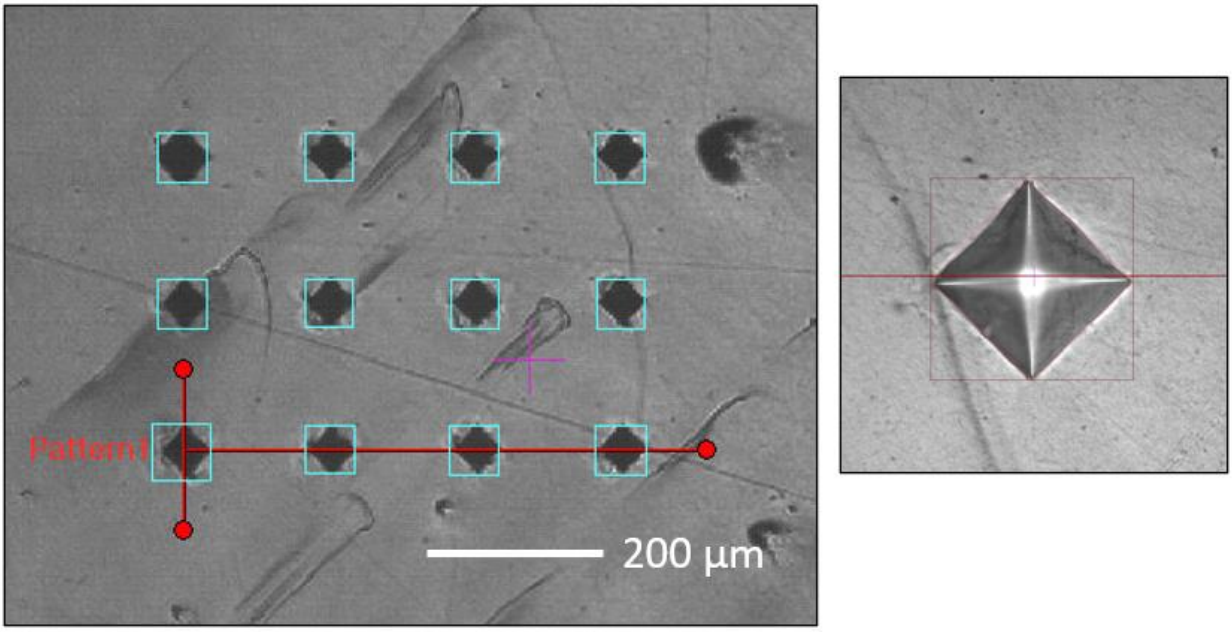

Figure 35. Vickers micro-hardness testing indention pattern on U-Nb-Zr as-cast sample.

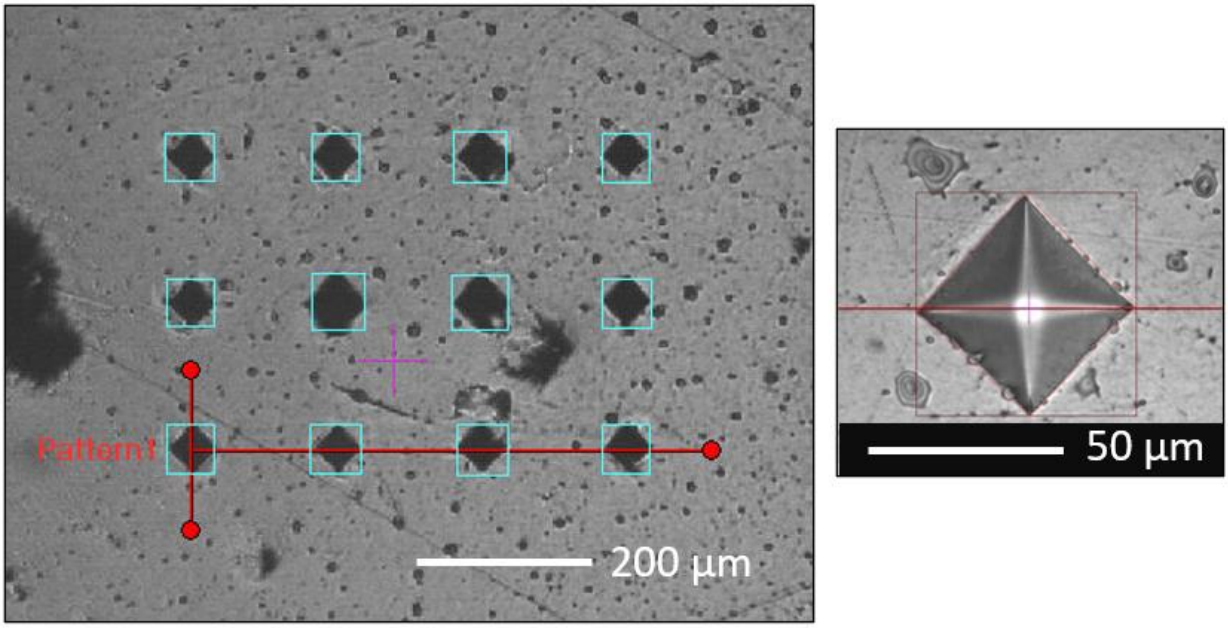

Figure 36. Vickers micro-hardness testing indention pattern on U-Nb-Zr (1200°C, 48 hour) sample.

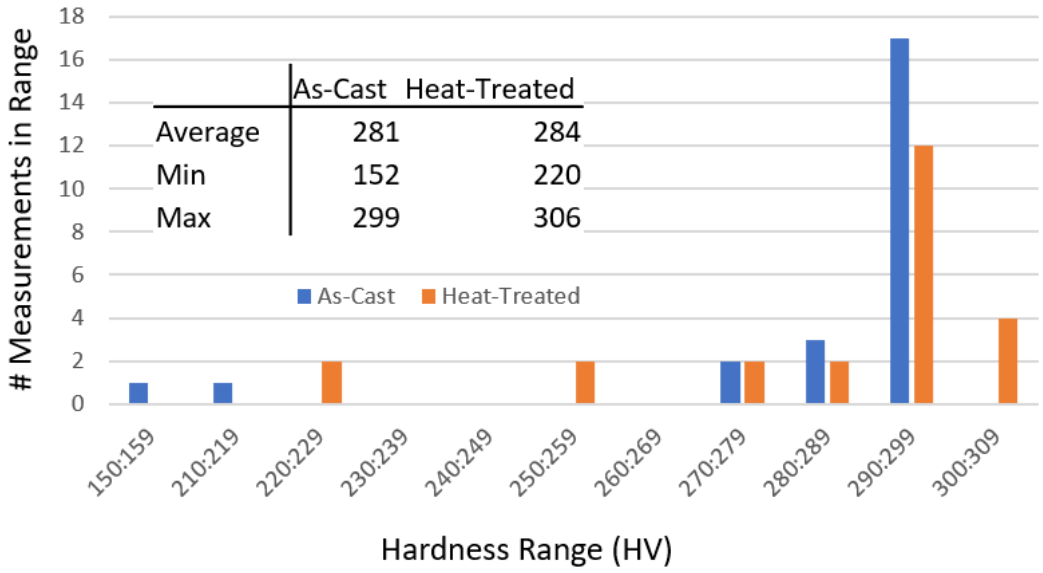

Figure 37. Distribution of Vickers micro-hardness testing measurements on U-Nb-Zr as-cast and heat-treated samples.

3.3 Fuel and Matrix Candidate Interaction Testing

3.3.1 Fuel: Matrix Interaction at 600ºC

Each fuel (U-10Mo, U-2Mo-1Si, U-1Mo-2Si) was tested against each matrix (U-43.28Nb-14.65Zr, Zr) candidate at 600ºC for 1 week as described in Section 1.1.4. The diffusion couples were mounted in the jigs to maintain pressure throughout the preparation and analysis. The fuel:matrix interface was analyzed via SEM, (and a representative region of each interface is shown in Figure 38. A significant gap was observed in one of the diffusion couples (U-2Mo-1Si:U-Nb-Zr) along the full length of the interface. It is unknown if the lack of contact is an effect of the assembly process and created insufficient contact for an interaction to occur, or if the gap was caused by separation of the sample materials during cooling. Regardless of the gap's time of occurrence, no evidence of interaction was observed between materials.

A gap was also observed along the full length of the U-10Mo:U-Nb-Zr diffusion couple interface. However variations along the edges of the samples were observed in the BSE image. EDS line scans across these regions, shown in Figure 39, exhibit a small spike in Nb approximately 0.5 µm into the U-Mo fuel. Since this spike does not correspond with an increase in the Mo signal, it is not suspected to be an artifact of the Nb-Mo peak overlap that causes the artificial increase of Mo signal in the U-Nb-Zr. This phenomenon is corrected for in the remaining samples to distinguish Mo from Nb as described in Section 1.1.4. This provides evidence that an interaction between the material occured and the samples separated upon cooling. Zirconium precipitates were also observed in clusters along the U-Nb-Zr side of the interface but were also observed in areas along the edge of the U-Nb-Zr sample that were not interfacing with the U-Mo sample. The appearance of the precipitates is therefore not likely to be a result of interaction.

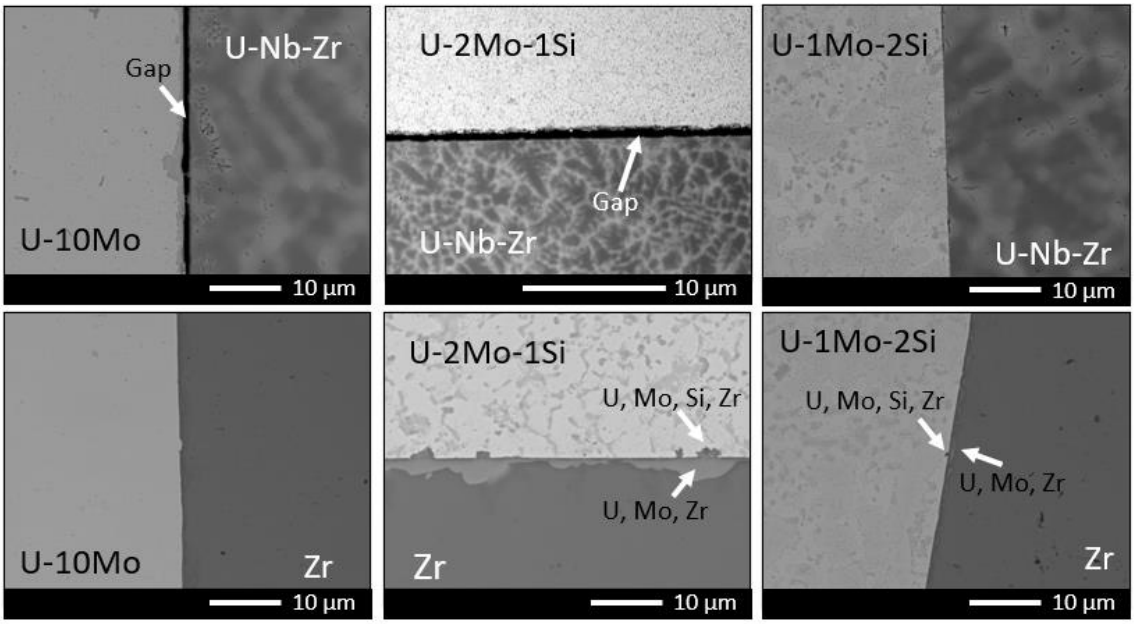

Figure 38. Comparison of Fuel:Matrix interactions at 600°C via BSE imaging.

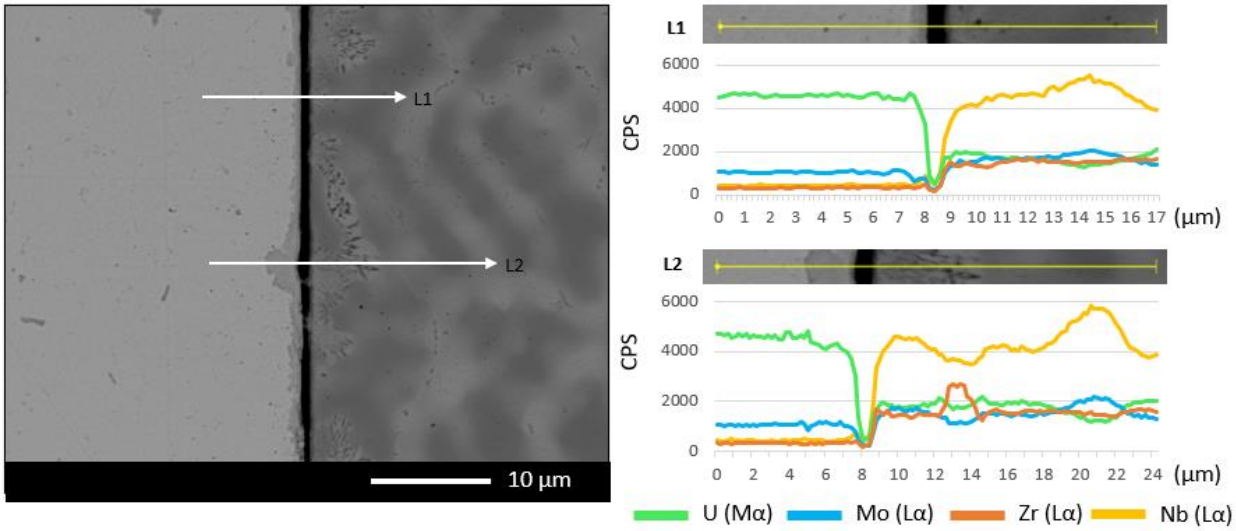

Figure 39. EDS line scans across the U-10Mo:UNbZr (600°C) interface

Small features were observed along the interface of the U-10Mo:Zr diffusion couple that appeared as light and dark variations along the Zr side of the interfaces, as shown in Figure 40. EDS line scans were collected across the interface where no feature (L1), a light feature (L2), and a dark feature (L3) was observed. However, the lines scans showed little variation between them. Due to the size of these features, minor variations in composition may not be distinguishable by this method. It was unable to be determined whether these features are evidence of interaction or unrelated surface artifacts.

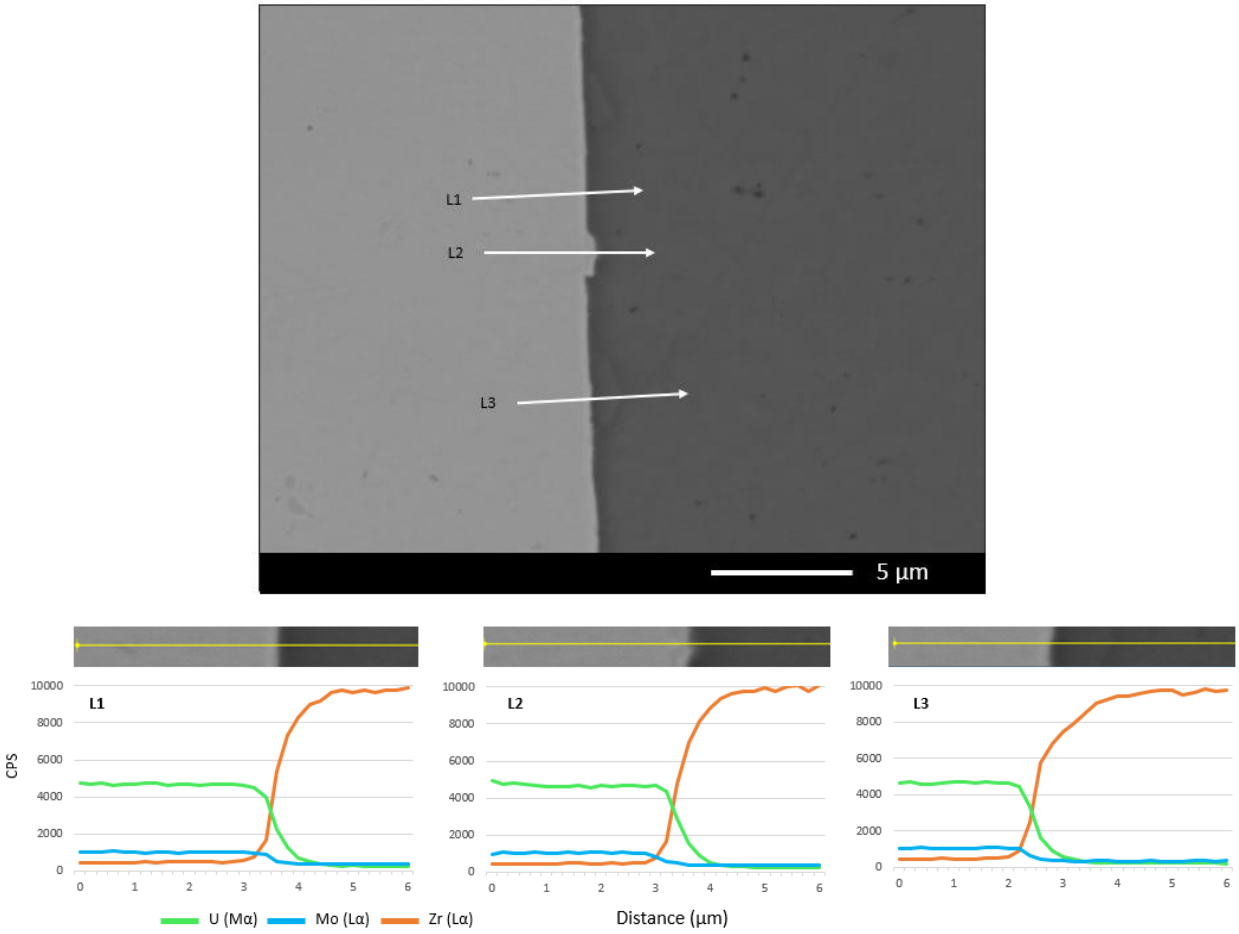

Figure 40. EDS line scans across the U-10Mo:Zr (600°C) interface.

The U-2Mo-1Si sample exhibited significant interaction behavior with the Zr matrix material. Along the interaction interface, regions contain U, Mo, and Zr can be observed in the Zr side of the interface, as indicated by point 1 in Figure 41. Although the thickness of this interaction varied, many interaction regions were up to 5µm thick. Smaller regions containing Zr can also be observed on the U-Mo-Si side of the interface.

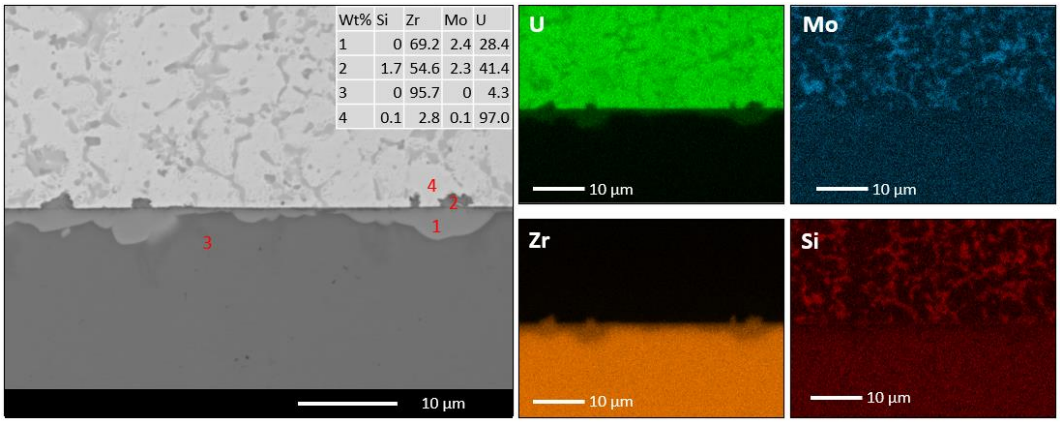

Figure 41. EDS map and point identification of U-2Mo-1Si:Zr (600°C) interface.

The U-1Mo-2Si also interacted with the Zr matrix material, though less significantly than the U-2Mo-1Si. One such example is shown in Figure 42, with EDS points measured showing areas contains U, Mo, and Zr along the boundary. The EDS map also indicated that a Si-rich layer may form along the boundary. The EDS maps were unable to distinguish variation in the Mo content, so the Mo map is not presented here. EDS line scans were performed across the interface at a region with no apparent interaction and a region with interaction. These lines scans, shown in Figure 43, show a difference in the Mo content along the boundaries of these two regions, by an increase in Mo for a 0.5-1 μm distance into the Zr. There is also increase in Si content (approximately 5 wt%) along the interface. In the region with Zr diffusion into the fuel sample, the Si-rich layer exists between the fuel and U-Mo-Zr interaction region rather than at the interface of the fuel and matrix as observed in the region with no interaction.

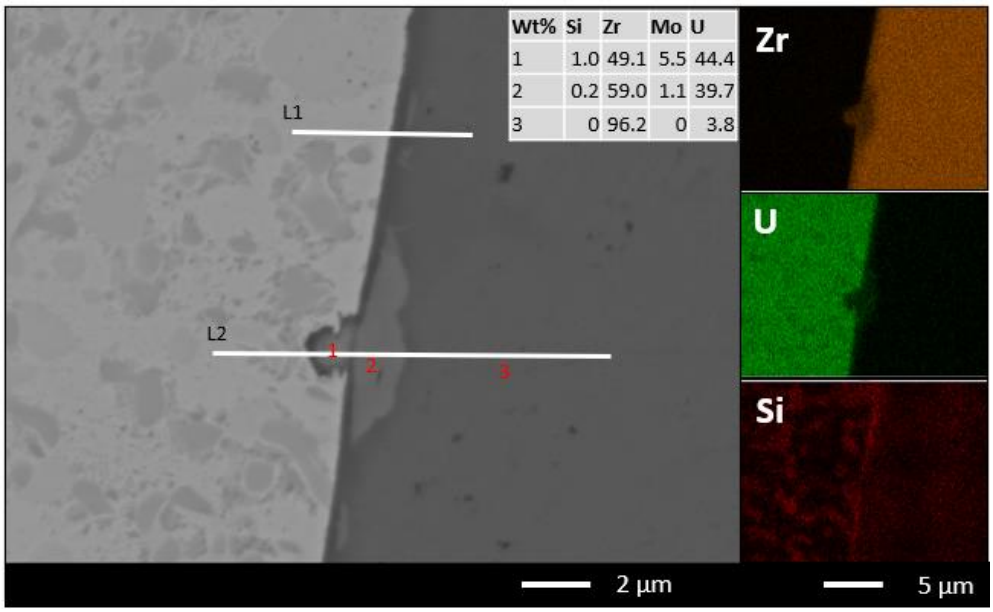

Figure 42. EDS map and point identification of U-1Mo-2Si:Zr (600°C) interface.

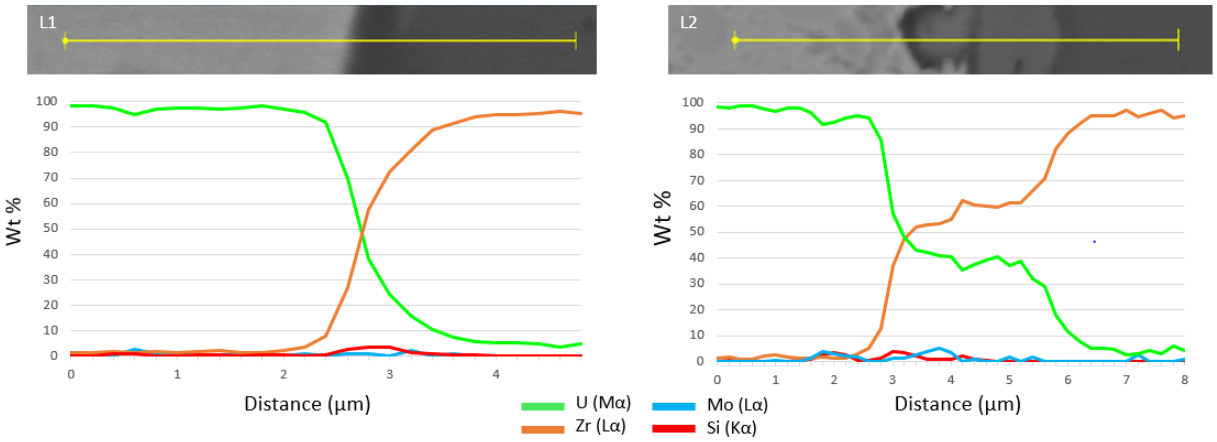

Figure 43. EDS Line scans of U-1Mo-2Si:Zr (600°C) interface.

No interaction was observed between the U-1Mo-2Si sample and the U-Nb-Zr matrix material, as shown in Figure 44. Due to significant peak overlap between Nb and Mo, the content of Mo qualitatively appeared higher in the U-Nb-Zr. This was corrected by using a single distinguishing Mo peak to identify Mo and generate the EDS map, as discussed in Section 2. However, due to the low signal of this peak, a significant content of Mo was unable to be distinguished.

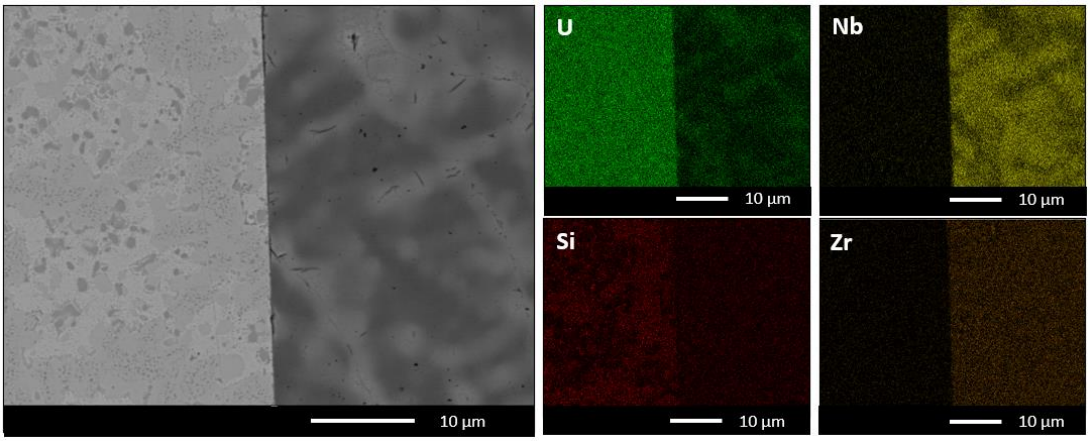

Figure 44. EDS maps of U-1Mo-2Si:UNbZr (600°C) interface.

3.3.2 Fuel:Matrix Interactions at 700ºC

Each fuel (U-10Mo, U-2Mo-1Si, U-1Mo-2Si) was tested against each matrix (U-43.28Nb-14.65Zr, Zr) candidate at 700ºC for 1 week as described in Section 1.1.4. The fuel:matrix interface was analyzed via SEM, and a representative region of each interaction is shown in Figure 45. Each of these interfaces exhibited regions with significant contact between the fuel and matrix samples and were analyzed in further detail.

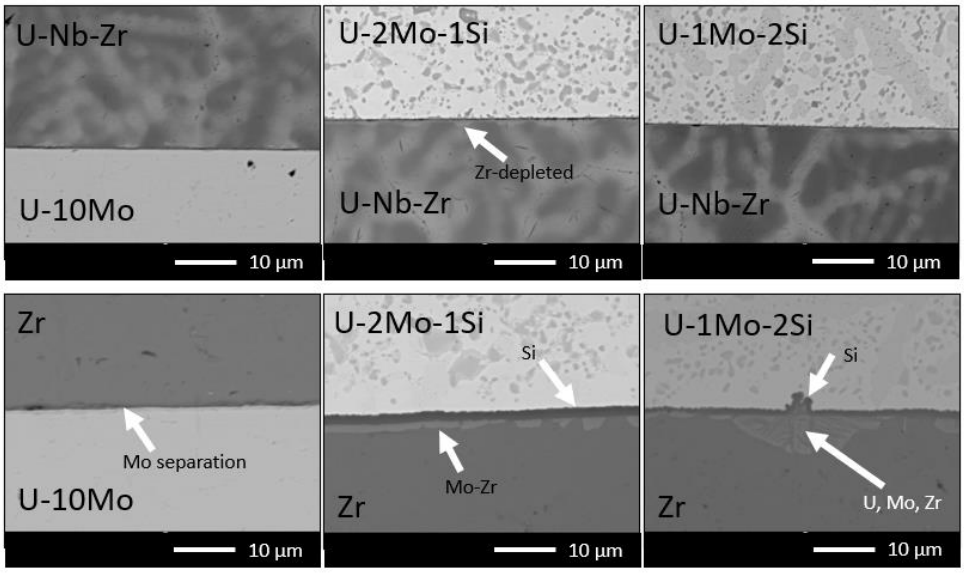

Figure 45. Comparison of Fuel:Matrix interactions at 700°C via BSE imaging.

A distinguishable interaction layer was not observed along the majority of the U-10Mo and Zr interface. However, small regions, such as that shown in Figure 46, did show minor separation of Mo from the U-Mo sample, most evident in the Mo EDS map. Minor diffusion between Mo and Zr may have occurred in these regions. The U-Nb-Zr sample showed no discernable evidence of an interaction with the U-10Mo fuel, as shown in the BSE image and EDS map in Figure 47. Due to significant peak overlap between Nb and Mo, the content of Mo qualitatively appeared higher in the U-Nb-Zr. This was corrected by using a single distinguishing Mo peak was used to identify Mo and generate the EDS map, as discussed in Section 2.

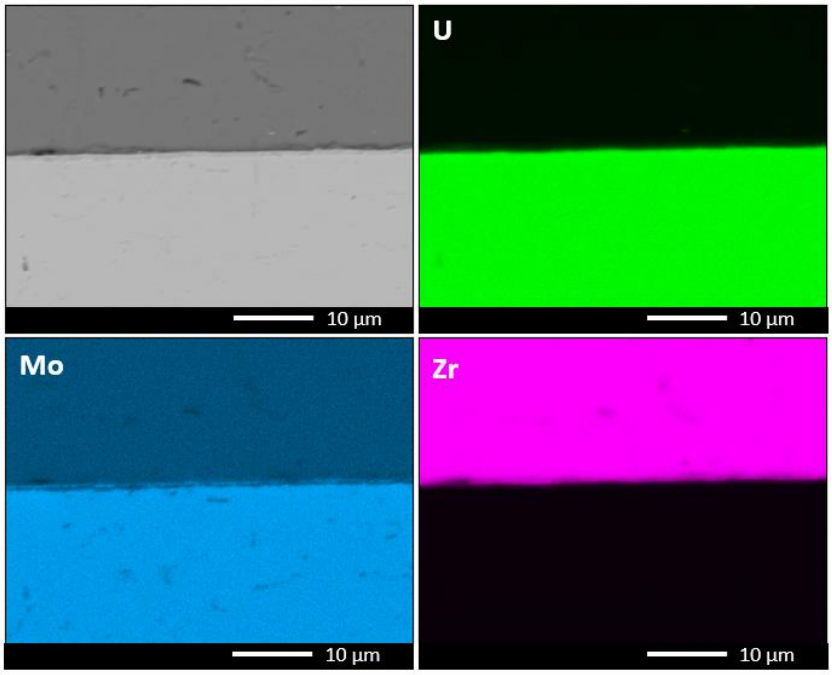

Figure 46. EDS maps of U-10Mo:Zr (700°C) interface.

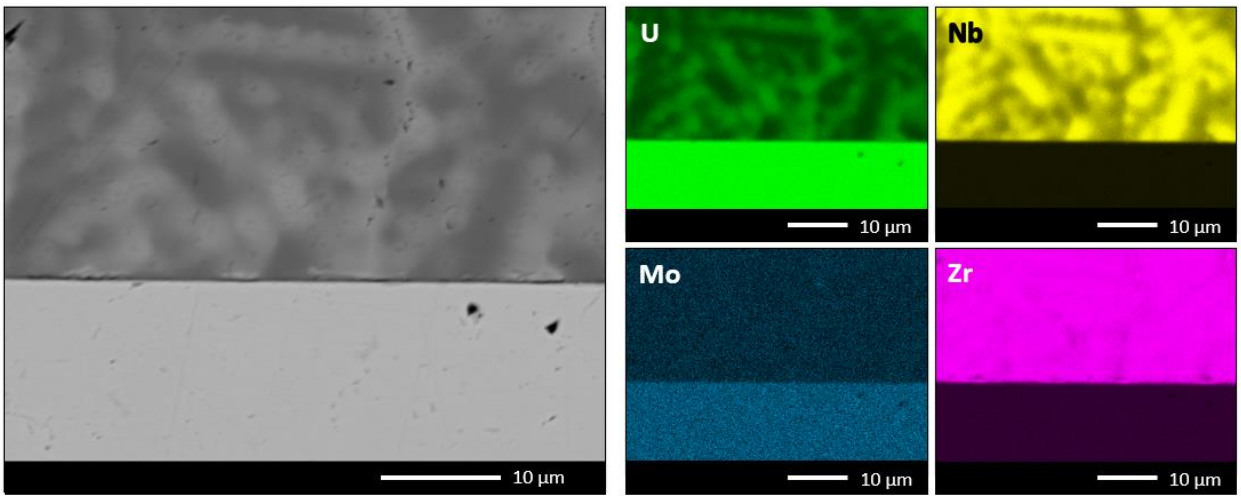

Figure 47. EDS maps of U-10Mo:U-Nb-Zr (700°C) interface.

The U-1Mo-2Si and Zr exhibited the most significant interaction of the fuel and matrix combinations at 700ºC. A thin Si-rich layer, as shown in the Si EDS map in Figure 48, was present along the length of the fuel-matrix interface. The EDS line scan, indicated by the white arrow in Figure 48, shows that U is also present in this layer, suggesting the formation of a U-Si layer of up to 3µm thick. Along the interface, there are regions of a U-Mo-Zr interaction on the Zr side of the U-Si layer. The most significant example of this interaction is shown in Figure 48, with the region reaching a thickness of 7µm and spanning across both sides of the interface. The primary interaction occurs between the U and Zr, with a secondary microstructure forming with alternating Zr-rich and U-rich lamella. Cooling from the solid solution may cause the formation alpha-Zr and delta-UZr2 phases though the actual mechanism for the formation of this interaction is undetermined [9].

The interaction test with U-1Mo-2Si and U-Nb-Zr produced a significantly different result. While the Mo signal had to be corrected and previously discussed, there was no evidence of an interaction between the fuel and matrix sample observed in the BSE images or EDS maps, shown in Figure 49.

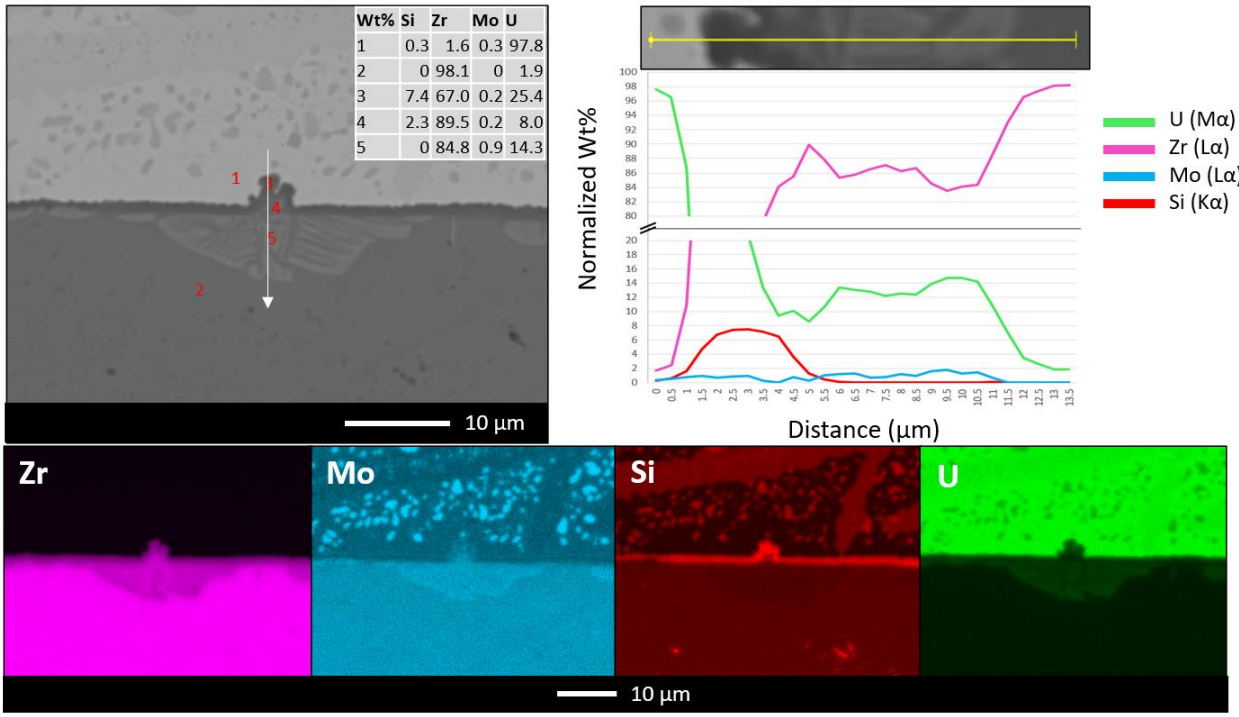

Figure 48. EDS maps, point identification, and line scan of U-1Mo-2Si:Zr (700°C) interface.

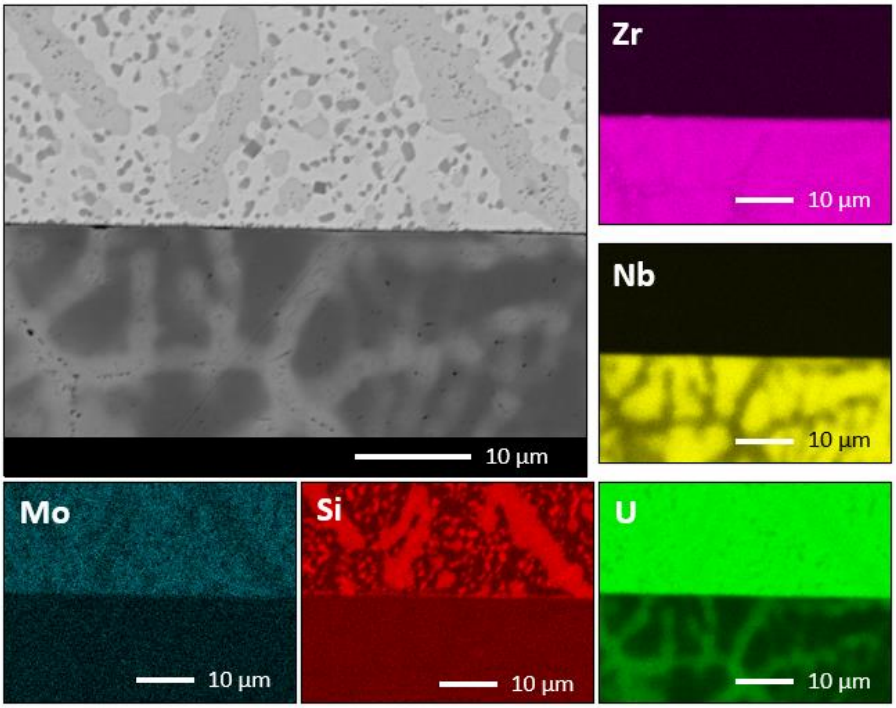

Figure 49. EDS maps of U-1Mo-2Si:UNbZr (700°C) interface.

The U-2Mo-1Si sample also exhibited a significant interaction with Zr after heating to 700ºC. A consistent U-Si-Zr layer (approximately 2 µm thick) was also observed along the interface, shown in Figure 50, similar to that observed along the U-1Mo-2Si:Zr interface. There were also U-Mo-Zr regions observed along Zr side of the interface, though none thick enough to observe the lamella secondary microstructure. The EDS point scan, indicated as point 1 in Fig. 50, consisted of a similar U concentration as that observed with the U-1Mo-2Si sample, but a higher Mo content. Since this corresponds with the higher content of Mo in this alloy, the presence of Mo may be due to Mo matrixed with U as opposed to a Mo-Zr eutectic.

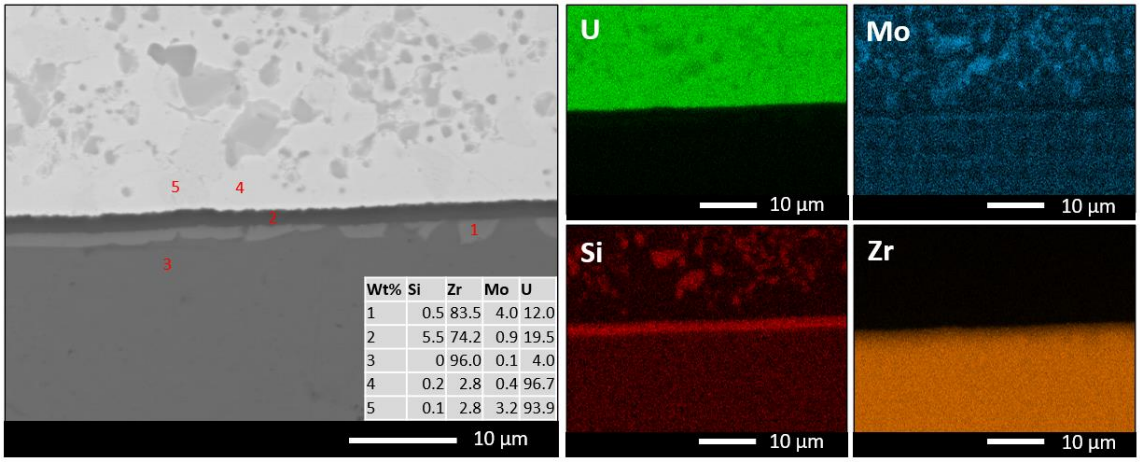

Figure 50. EDS maps of U-2Mo-1Si:Zr (700°C) interface.

There were no observable regions of inter-diffusion between the U-2Mo-1Si fuel and U-Nb-Zr matrix samples. The Mo EDS map was corrected to distinguish from Nb, as previously discussed to generate the maps shown in Figure 51. The BSE image did show some varying regions along the matrix side of the interface. The EDS maps were unable to resolve a variation in composition, so two EDS line scans were analyzed. L1 (Figures 51 and 52) corresponded to a region with minimal variation and L2 corresponded to a region where variation was observed. L2 showed a decrease in the normalized weight concentration of Zr through this region (between locations 3.5 and 5 µm) that was not observed in L1. The cause of the depletion of Zr in the region was not determined in this study.

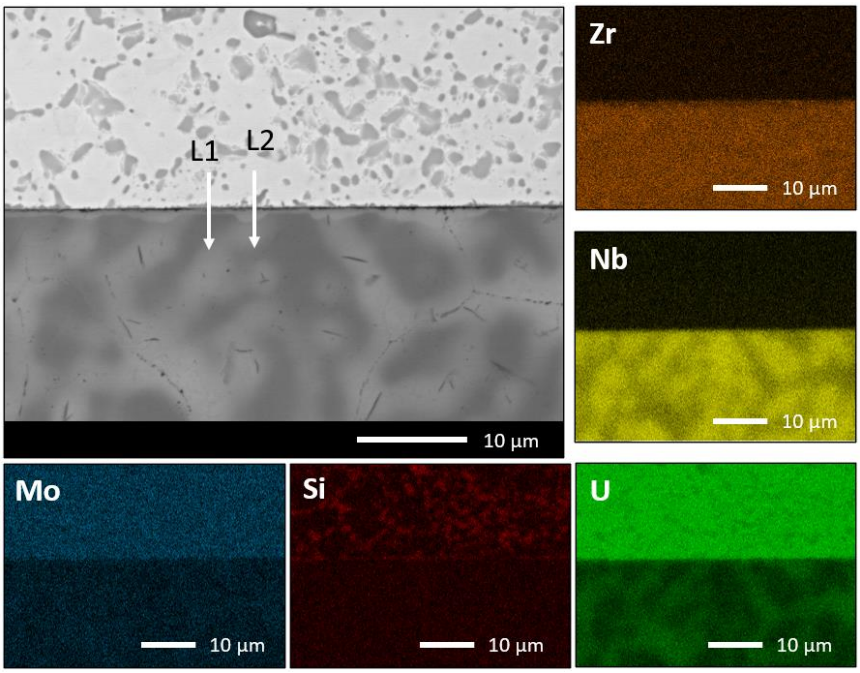

Figure 51. EDS maps of U-2Mo-1Si:UNbZr (700°C) interface.

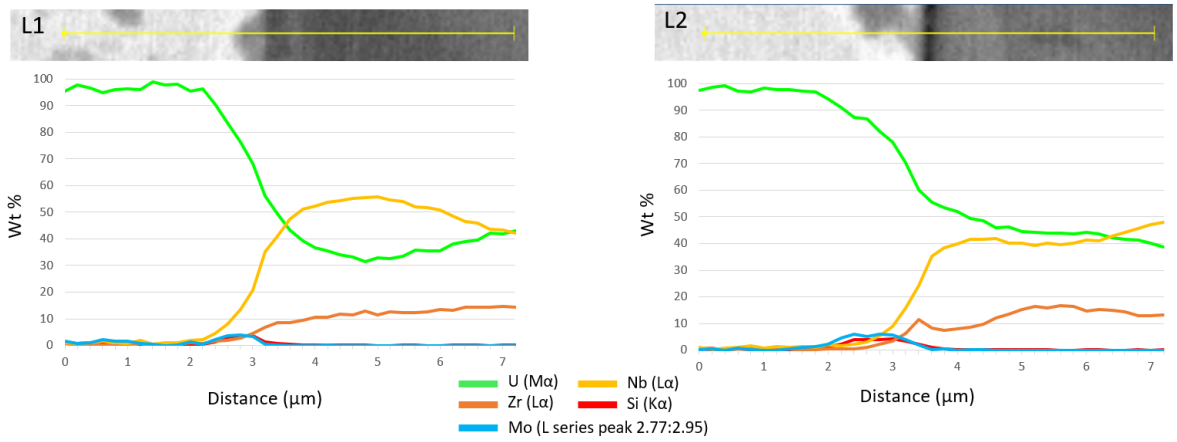

Figure 52. EDS line scans of U-2Mo-1Si:UNbZr (700°C) interface.

4. CONCLUSIONS

4.1 Advanced Alloy Characterization

Advanced fuel candidates were fabricated and characterized in effort to produce single-phase alloy systems. The U-xMo-ySi fuel candidates were unable to be fabricated as single-phase systems. Although the phase structure in as-cast samples varied throughout the sample, the phases became more discreet and consistent following heat treatment at elevated temperatures. Quenching of these samples in a water bath had no significant effect on the resulting microstructure, failing to prevent the formation of additional phases during cooling. These initial difficulties reduced the interest in this fuel system as a viable option and was not further studied. Additional testing would be required to produce single-phase systems. As-cast samples of U-4Si, with a target phase of U_3Si, also showed a multitude of phases present throughout the samples of multiple casting attempts. Heat-treatment testing on this candidate would be required to study the phase formation at different temperatures.

Heat-treatment of the U-43.28Nb-14.65Zr alloy yielded more successful homogenization results. Although the casting process resulted in the formation of a distinct Nb-rich dendritic structure, a single-phase bulk structure formed after heating the samples at 1200ºC for 48 hours. Zirconium precipitates formed within the bulk material but did not show a significant impact on the overall phase structure of the alloy. Heating samples for longer periods of time did not significantly impact the overall microstructure, showing phase restructuring occurred within 48 hours at the target temperature. The DSC and specific heat curves provided additional evidence of a non-reversible phase change starting around 1050ºC. The homogenization of the multi-phase as-cast samples is expected to improve the irradiation behavior of the system, although additional pre- and post-irradiation testing would be needed to examine the behavior of this alloy system in the anticipated range of operating temperature. Additional work would also include evaluation of thermal expansion to develop the thermal conductivity as a function of temperature.

4.2 Fuel:Matrix Interactions

Fuel candidates (U-xMo, U-1Mo-2Si, U-2Mo-1Si) were tested against matrix candidates (Zr, U-43.28Nb-14.65Zr) to examine interaction behavior at elevated temperatures. Comparing the interaction behavior at 600ºC is incomplete due to gaps between samples. Both U-xMo-ySi alloys demonstrated significant interaction with the Zr matrix, while the U-1Mo-2Si did not interact with the U-Nb-Zr.

The 700ºC test was a more comprehensive comparison of the interaction behaviors among the candidate alloys. Since this test was performed above the intended operation temperature range, the results of this test may only be representative for potential temperature fluctuations from the intended operating range. Both U-xMo-ySi alloys showed increased interaction with the Zr fuel from the 600°C test and showed additional formation of layers and secondary microstructures within the interaction regions. The formation of a U-Si layer on the fuel side and U-Mo-Zr regions on the matrix side of the interface represented the complexity of the interaction introduced with a ternary fuel system, but no significant interaction was observed with the U-Nb-Zr matrix. The U-10Mo fuel sample provided evidence of a minor interaction with Zr, but none was observed with the U-Nb-Zr.

Overall, the U-43.28Nb-14.65Zr matrix demonstrated improved compatibility with all fuel candidates. In both tests, U and Mo components were more likely to diffuse into a Zr matrix than a U-Nb-Zr matrix. This phenomenon being more pronounced in Si-bearing fuels.

5. REFERENCES

1. Pasqualini, E.E., et al., *Fabrication and testing of U–7Mo monolithic plate fuel with Zircaloy cladding.* Journal of Nuclear Materials, 2016. **479**: p. 402-410.
2. Robinson, A.B., et al., *Irradiation Performance of U-Mo Alloy Based 'Monolithic' Plate-Type Fuel – Design Selection*. 2009: United States.
3. Meyer, M.K., et al., *Low-temperature irradiation behavior of uranium–molybdenum alloy dispersion fuel.* Journal of Nuclear Materials, 2002. **304**(2): p. 221-236.
4. "Development status of metallic, dispersion and non-oxide advanced and alternative fuels for power and research reactors," IAEA-TECDOC-1374, International Atomic Energy Agency, Vienna, Austria, 2003.
5. Zhou, P., et al., *Thermodynamic modeling of the U-Nb-Zr ternary system.* Journal of Nuclear Materials, 2019. **523**: p. 157-171.
6. Okamoto, H, *Si-U (Silicon-Uranium).* Binary Aloy Phase Diagrams, II edition, 1990.
7. Rogl, P., et al., *Phase equilibria and magnetism in the Mo-Si-U system.* Journal of Nuclear Materials, 2001. **288**(1)L p. 66-75.
8. Ewh, A., et al., *Microstructural characterization of U-Nb-Zr, U-Mo-Nb, and U-Mo-Ti alloys via electron microscopy.* Journal of Phase Equilibria and Diffusion, 2010. **31**(3): p. 216-222.
9. Kurata, M., et al., *Thermodynamic assessment of the Fe-U, U-Zr, and Fe-U-Zr systems.* Journal of Alloys and Compounds, 1998. **271-273**: p. 636-640.